U.S. DEPARTMENT OF THE INTERIOR
U.S. GEOLOGICAL SURVEY

Prepared in cooperation with the CITY OF WILLIAMS

Structural Controls on Ground-Water Conditions and Estimated Aquifer Properties near Bill Williams Mountain, Williams, Arizona

Water-Resources Investigations Report 01—4058

USGS
science for a changing world

U.S. DEPARTMENT OF THE INTERIOR
U.S. GEOLOGICAL SURVEY

Structural Controls on Ground-Water Conditions and Estimated Aquifer Properties near Bill Williams Mountain, Williams, Arizona

By Herbert A. Pierce

Water-Resources Investigations Report 01—4058

Prepared in cooperation with the
CITY OF WILLIAMS

Tucson, Arizona
2003
(First printing, 2001)

U.S. DEPARTMENT OF THE INTERIOR
GALE A. NORTON, Secretary

U.S. GEOLOGICAL SURVEY
Charles G. Groat, Director

For additional information write to:

District Chief
U.S. Geological Survey
Water Resources Division
520 N. Park Avenue, Suite 221
Tucson, AZ 85719–5035

Copies of this report can be purchased from:

U.S. Geological Survey
Information Services
Box 25286
Federal Center
Denver, CO 80225–0046

Information about U.S. Geological Survey programs in Arizona is available online at http://az.water.usgs.gov.

CONTENTS

FIGURES

TABLES

CONVERSION FACTORS AND DATUMS

Multiply	By	To obtain
millimeter (mm)	0.03937	inch
meter (m)	3.281	foot
kilometer (km)	0.6214	mile
square kilometer (km^2)	247.1	acre
liter per second (L/s)	15.85	gallon per minute
square meter (m^2)	10.76	square foot
radian (rad)	0.017453	degree
milligal (mGal)	.00001	Gal

Temperature in degrees Celsius (°C) may be converted to degrees Fahrenheit (°F) as follows:

$$°F = 1.8(°C)+32$$

Sea level: In this report, "sea level" refers to the National Geodetic Vertical Datum of 1929 (NGVD of 1929)—A geodetic datum derived from a general adjustment of the first-order level nets of the United States and Canada, formerly called Sea Level Datum of 1929. **Altitude**, as used in this report, refers to distance above or below sea level.

ABBREVIATED WATER-QUALITY UNITS

Chemical concentration and water temperature are given only in metric units. Chemical concentration in water is given in milligrams per liter (mg/L) or micrograms per liter (μg/L). Milligrams per liter is a unit expressing the solute mass (milligrams) per unit volume (liter) of water. One thousand micrograms per liter is equivalent to 1 milligram per liter. For concentrations less than 7,000 milligrams per liter, the numerical value is about the same as for concentrations in parts per million. Specific conductance is given in microsiemens per centimeter at 25 degrees Celsius (μS/cm at 25°C).

ABBREVIATED GEOPHYSICAL TERMS

Ampere is the International System (S.I.) unit of electric current measured as one coulomb per second or one volt per ohm. Ohm is the International System unit of electrical resistance equal to that of a conductor in which a current of one ampere is produced by a potential of one volt across its terminals. Ohm meter (Ω•m) is a unit of resistivity, also written as ohm meter squared per meter ($\Omega \bullet m^2/m$), and is the resistance of a meter cube to the flow of current between opposite faces. Farad is the International System unit of capacitance equal to the capacitance of a capacitor having a charge of 1 couloumb on each plate and a potential difference of 1 volt between the plates. Henry is the International System unit of electrical inductance in which an induced electromotive force of one volt is produced when the current is varied at the rate of one ampere per second. Radian is a unit of angular measure equal to the angle subtended at the center of a circle by an arc of length equal to the radius of the circle. Gamma is a unit of magnetic field equal to one nanotesla, the preferred International System name (1 gamma=10^{-5} gauss=10^{-9} tesla). Milligal (mGal) is a unit of acceleration used in gravity field measurements. Hertz is a unit of frequency equal to one cycle per second. Kilohertz is a unit of frequency equal to 1,000 hertz. The weber is the magnetic flux which, linking a circuit of one turn, produces in it an electromotive force of one volt as it is reduced to zero at a uniform rate in one second.

Structural Controls on Ground-Water Conditions and Estimated Aquifer Properties near Bill Williams Mountain, Williams, Arizona

By Herbert A. Pierce

Abstract

As of 1999, surface water collected and stored in reservoirs is the sole source of municipal water for the city of Williams. During 1996 and 1999, reservoirs reached historically low levels. Understanding the ground-water flow system is critical to managing the ground-water resources in this part of the Coconino Plateau. The nearly 1,000-meter-deep regional aquifer in the Redwall and Muav Limestones, however, makes studying or utilizing the resource difficult.

Near-vertical faults and complex geologic structures control the ground-water flow system on the southwest side of the Kaibab Uplift near Williams, Arizona. To address the hydrogeologic complexities in the study area, a suite of techniques, which included aeromagnetic, gravity, square-array resistivity, and audiomagnetotelluric surveys, were applied as part of a regional study near Bill Williams Mountain. Existing well data and interpreted geophysical data were compiled and used to estimate depths to the water table and to prepare a potentiometric map. Geologic characteristics, such as secondary porosity, coefficient of anisotropy, and fracture-strike direction, were calculated at several sites to examine how these characteristics change with depth.

The 14-kilometer-wide, seismically active northwestward-trending Cataract Creek and the northeastward-trending Mesa Butte Fault systems intersect near Bill Williams Mountain. Several north-south-trending faults may provide additional block faulting north and west of Bill Williams Mountain. Because of the extensive block faulting and regional folding, the volcanic and sedimentary rocks are tilted toward one or more of these faults. These faults provide near-vertical flow paths to the regional water table. The nearly radial fractures allow water that reaches the regional aquifer to move away from the Bill Williams Mountain area.

Depth to the regional aquifer is highly variable and depends on location and local structures. On the basis of interpreted audiomagnetotelluric and square-array resistivity sounding curves and few well data, depths to water may range from 450 to 1,300 meters.

INTRODUCTION

Currently (1999), the city of Williams, Arizona, supplies its residents with water exclusively from surface reservoirs. During periods of drought, surface runoff is negligible or may not occur at all. Infiltration and evaporation reduce runoff from Bill Williams Mountain and further reduce reservoir storage once the water is contained in the reservoirs. Most of the reservoirs have been lined to reduce infiltration, however, evaporation continues to reduce storage.

Population growth and the drought of 1995–96 prompted the city to explore the possibility of using ground water as a backup to the surface-water system. Few wells have been drilled because the depth to water in this part of northern Arizona is nearly 1,000 m. The lack of wells limits the knowledge of the hydrogeology of the regional ground-water system.

Williams is near the intersection of two roughly orthogonal fault systems (**fig. 1**). The fault systems are wide zones of subparallel faults. The fault zones (Mesa Butte and Cataract Creek Fault systems) intersect at

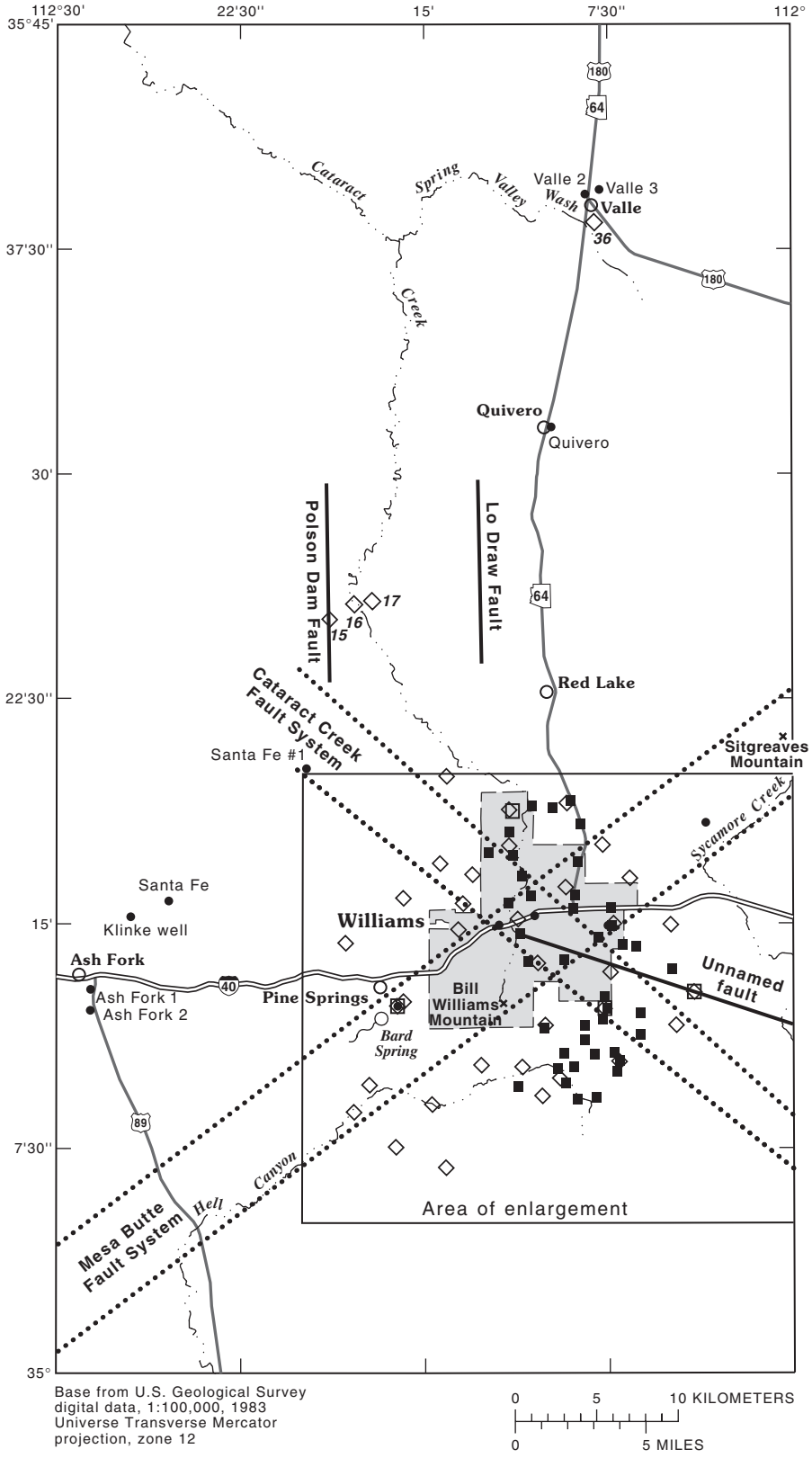

Figure 1. Location of study area and locations of wells, selected springs, gravity stations, audiomagnetotelluric sites, square-array resistivity sites, and faults and fault systems near Williams, Arizona.

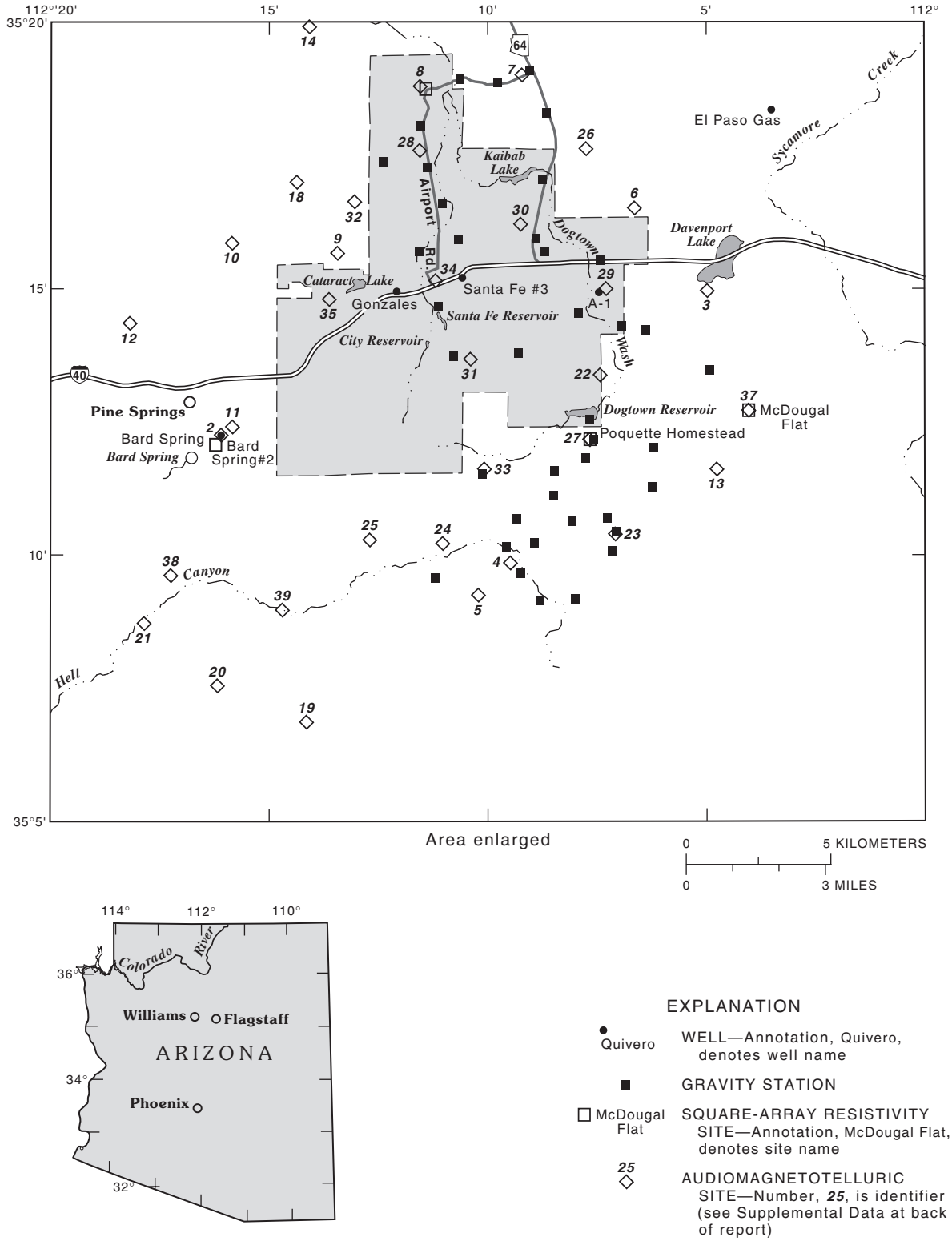

Figure 1. Continued.

Bill Williams Mountain and create a weak spot in the crust as reflected by the volcanic activity of Tertiary age (Newhall and others, 1987). These fault systems are near-vertical faults zones, are seismically active (Shoemaker and others, 1978), and probably provide conduits for water from the near surface to the regional aquifer. This study by the U.S. Geological Survey (USGS), in cooperation with the city of Williams, was done during 1995–99 to provide information about the structure, lithology, and flow system of the regional aquifer.

This report was revised in March 2003 to eliminate minor editorial errors that were detected following the first printing in 2001. Fault labels and lines shown on figures 5, 6, 9, and 10 were revised to match the discussions of these figures in the text. In addition, figures 14 and 15 and the azimuth plots in figures 16–19 were revised to show only data points, and the water-level altitude for the A-1 well was revised to the correct value of 1,178 m. No changes, however, were made to the interpretations presented in the report.

Purpose and Scope

This report describes the hydrogeologic units and ground-water conditions in the regional aquifer near Williams, Arizona, identifies regional geologic structural features that in part control ground-water conditions in the regional aquifer, and presents estimated properties of the regional aquifer determined from surface-geophysical surveys. This study included reviews of previous geologic and hydrologic studies, databases, and published geologic information. In addition, geophysical data, digital elevation models (DEMs), aerial photography, and Thematic-Mapper (TM) images were analyzed. A shallow well was drilled and logged on the west side of Bill Williams Mountain. In addition, data were collected from 30 gravity stations, 13 scalar audiomagnetotelluric (AMT) soundings, 25 tensor AMT soundings, and 4 square-array direct-current resistivity (SAR) soundings. Data from the geophysical investigations provided information about local faults and provided the basis for estimates of depth to the water table.

Physical Setting

Williams is in north-central Arizona near the southern edge of the Colorado Plateau. Within the 2,510-km^2 study area, altitudes range from 1,981 m along Cataract Creek to 2,821 m at the top of Bill Williams Mountain. Bill Williams Mountain is near the western edge of the San Francisco volcanic field. This volcanic field along the southern edge of the Colorado Plateau is predominantly basaltic in composition. The basalt flows bury an erosional surface of Tertiary age, which cuts across a sedimentary sequence of Paleozoic age that is composed of limestone, dolomite, dolomitic limestone, dolomitic sandstone, sandstone, and mudstone. Near the study area, rocks of Paleozoic age are about 975 to 1,128 m thick. Along the southern edge of the Colorado Plateau, the Paleozoic rocks are as much as 1,524 m thick. Beneath the consolidated Paleozoic sediments are undifferentiated rocks of Proterozoic age that include granites, metavolcanics, and gneisses.

In and near the study area, the western edge of the San Francisco volcanic field generally is coincident with the western flank of the Kaibab Uplift. This uplift forms a broad, low, domal upwarp (**fig. 2**). The upwarp trends approximately north-south from the Williams-Flagstaff area to the Kaibab Plateau north of Grand Canyon. South of Grand Canyon, the uplift is called the Coconino Plateau. The San Francisco volcanic field and the Coconino Plateau are part of the 2,134-meter-high Kaibab Uplift. A few miles west of Williams, the San Francisco volcanic field and the Kaibab Uplift end, and the general altitude of the Colorado Plateau drops off abruptly to an average altitude of about 1,520 m.

The Colorado River is the largest surface-water feature near the study area (**fig. 3**). To the north and northwest of the study area, the Colorado River flows from east to west, then southwest and divides and drains the Coconino and Kaibab Plateaus. To the west and south, Chino Wash and the Verde River flow southeast and then south into the Phoenix area where they join the Salt River. To the east, the Little Colorado River flows northwestward to its confluence with the Colorado River.

Cataract Creek is the main drainage in the study area and is a major influence on the hydrogeology of the region. Although Cataract Creek is ephemeral for much of its course, the coincident fault zone and ancillary structures funnel ground water to the northwest toward Havasu Spring, which is the terminus of the Cataract Creek Fault system. Havasu Spring is the major ground-water discharge point for the western half of the Coconino Plateau. Several reservoirs on Cataract Creek and its tributaries serve as the municipal water supply for Williams.

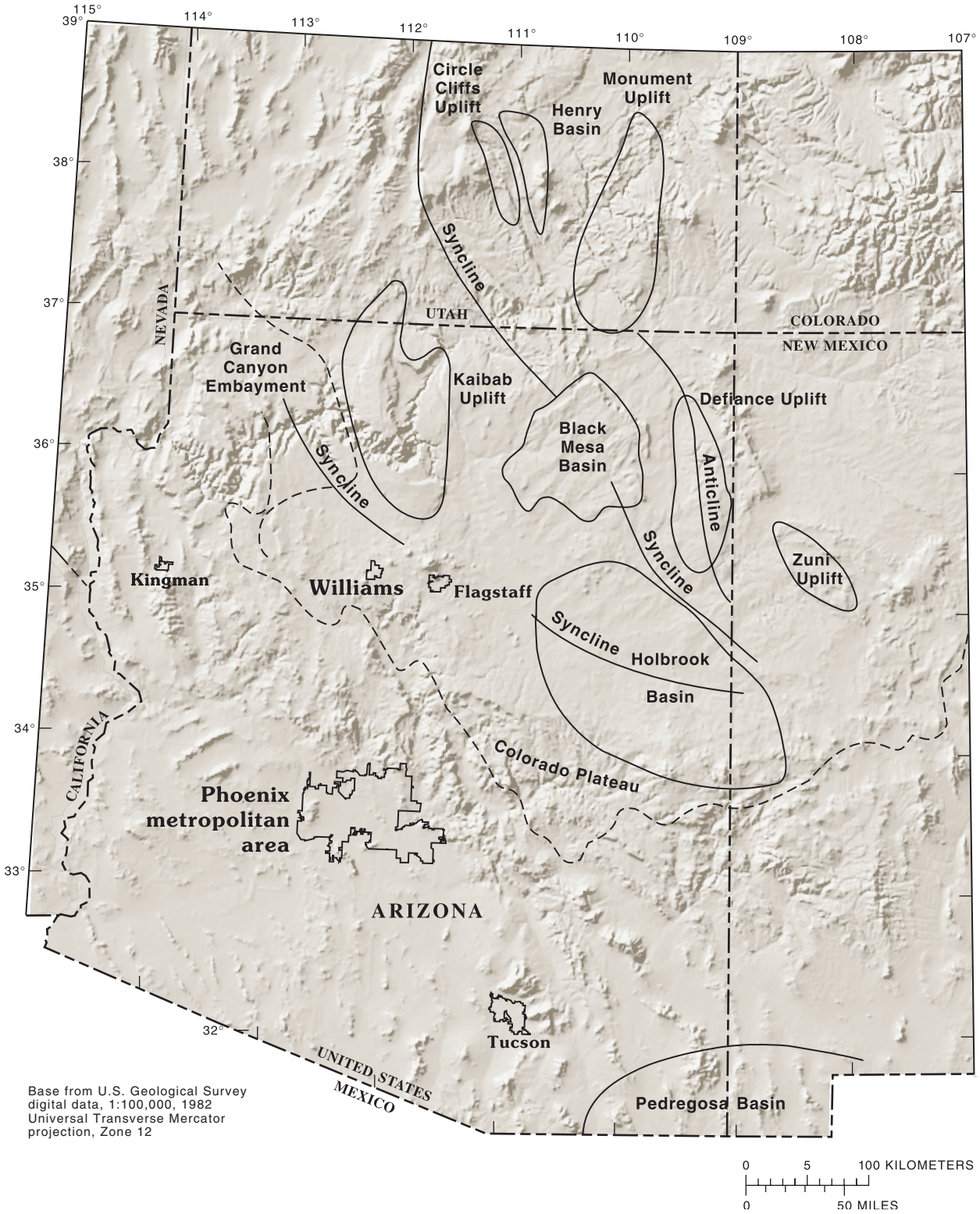

Figure 2. Laramide folds in Cretaceous rocks on the southwestern flank of the Colorado Plateau. The Kaibab Uplift and a synclinal feature associated with the Grand Canyon Embayment are two geologic features that affect ground-water flow near Williams, Arizona.

Figure 3. Overview of southwestern edge of the Colorado Plateau, Mogollon Rim, and Grand Canyon, and location of surface waters bounding the study area in northern Arizona.

The average monthly temperature varies with altitude. In Williams, average monthly temperatures range from 1.0°C in January to about 20.3°C in July, and average monthly temperature extremes range from -5.6°C to 28.1°C in January and July, respectively (National Climatic Data Center, NOAA, accessed June 2000). Precipitation in this cold, temperate climate is sufficient to support large stands of yellow pines and aspen groves in high, wet areas and piñon-juniper trees and meadow grasses in the lower and drier areas.

Williams has two wet seasons each year—December to March and July to August. Reservoir recharge occurs during March and April when the rains melt the snowpack. Williams receives an average of 560 mm of precipitation each year, but the amount can vary considerably from year to year (**fig. 4**).

The San Francisco Peaks volcanic field near Williams mantles the area and fills older valleys with volcanic deposits of Tertiary age (Damon and others, 1974). Bill Williams Mountain is near the intersection of Mesa Butte, Cataract Creek, and Lo Draw Faults. Volcanic rocks cover the faults but postdepositional

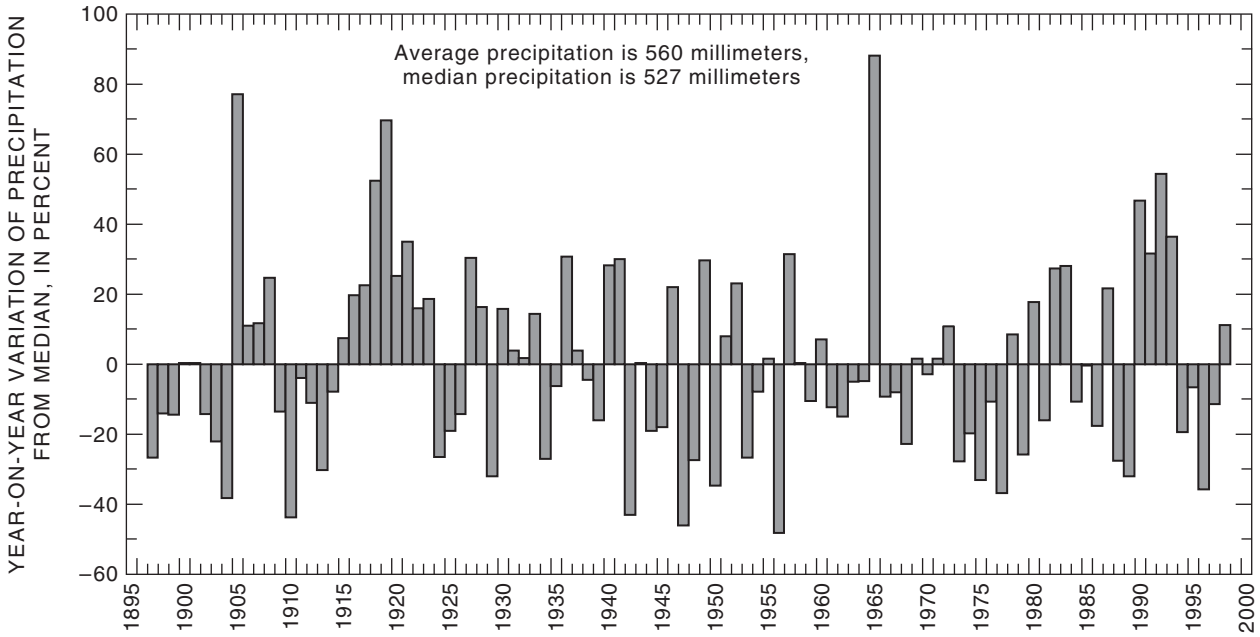

Figure 4. Variation in annual precipitation, city of Williams, Arizona, 1897–1998. The mean monthly precipitation was used for any month with 26 or more days of missing record, and a yearly total then was calculated. (Western Region Climate Center database, accessed 1996; data for 1996–98 from National Climatic Data Center, 1996–98).

deformation from seismic activity on the near-vertical and throughgoing Mesa Butte and Cataract Creek Fault systems is observable (Shoemaker and others, 1978). Northwest of Williams, the Cataract Creek Fault system trends southeast-northwest and forms a graben. The volcanic rocks cover the graben within the study area and thin to extinction to the north and northwest.

Previous Investigations

The city of Williams and the USGS have cooperated on water-resources projects since the early 1960s. Data from streamflow-gaging stations and crest-stage gages provided some of the first long-term information for the Dogtown Reservoir and Kaibab Lake on the Dogtown Wash drainage 7 km southeast and 5 km northeast of Williams, respectively. Thomsen (1969) completed a surface-water study near Williams, and although the primary focus of that study was surface water, Thomsen observed high rates of infiltration and evaporation in and around Williams. The porous and extensively fractured volcanic rocks provide a path to the underlying fractured consolidated sediments of the Coconino Plateau. Detailed descriptions of the geology of the study area are available in Darton (1910), McKee (1938, 1954), Metzger (1961), Shoemaker and others (1978), Blakey (1979, 1990), Billingsley and others (1980), Ulrich and others (1984), Blakey and Knepp (1989), and Sorauf and Billingsley (1991).

Errol L. Montgomery and Associates, Inc. (1996) assessed hydrogeologic conditions on the Coconino Plateau and defined a north-northwestward-trending oblate structural subbasin that begins near Williams on the south and trends north to the south rim of Grand Canyon. They defined the subbasin using many of the northwestward-, northeastward-, and northward-trending geologic structures mapped by Breed and others (1986), Billingsley and Huntoon (1983), Huntoon and Billingsley (1981), Loughlin and Huntoon (1983), and Shoemaker and others (1978). Errol L. Montgomery and Associates, Inc. (1996) grouped the Redwall Limestone, Temple Butte Formation, and the Muav Limestone within the subbasin into a single geohydrologic unit called the Redwall-Muav aquifer. Thiele (1964a, b) assessed the deep aquifers. The interpreted geophysical curves did not indicate methods used or provide original data; therefore, the curves were not used in this study.

METHODS OF INVESTIGATION

Gravity and magnetic-potential field methods were used to identify variations in rock density and magnetic susceptibility. The objective was to associate density and magnetic-field variations with differences in the areal and vertical distribution of rock types and structures. A TM image, aerial photographs, and a DEM were used to complement observations from the geology, hydrology, and potential-field data. The large spatial coverage provided by these data sets allowed an overview of the study area and information on large-scale regional structures. Square-array and electromagnetic soundings provided information on the subsurface-resistivity structure and estimates of depths to the water table.

Well data were collected and used to provide ground truth and augment the interpreted depth-to-water estimates generated by the soundings. During the course of the study, a well, Bard Spring #2, was drilled on the west side of Bill Williams Mountain. Geophysical and lithologic logs were compiled from Bard Spring #2 and were used to provide ground truth for electrical soundings on the west side of the study area.

Gravity Measurements

Gravity measurements were made at 40 sites near the intersection of the Mesa Butte and Cataract Creek Fault systems (**fig. 1**) to supplement the gravity data taken from the USGS 2-km simple Bouguer gravity-data grid (Phillips and others, 1993). Gravity measurements were made using a LaCoste & Romberg Model D gravity meter (Model D-76) with loops back to the USGS absolute-gravity station (WaltBM) in Flagstaff. These new data were merged with the existing data set and then plotted (**fig. 5**). The data provide improved resolution on the gravity-anomaly map for the area southeast of Williams near the intersection of the Mesa Butte and Cataract Creek Fault systems.

Aeromagnetic Measurements

The aeromagnetic data (for 2,134 km^2) used in this survey were extracted from the United States 2-km grid of the USGS (Phillips and others, 1993), converted to a Universal Transverse Mercator (UTM) projection, and contoured every 50 gammas (**fig. 6**). Aeromagnetic surveys measure magnetic field anomalies caused by changes in the magnetic fields of geological bodies that are superimposed on the Earth's magnetic field. The magnetic effects of a rock, or the intensity of magnetization, is complex in that it has a magnitude and a direction. In aeromagnetic prospecting, variations in the intensity of some component of the field usually are measured. After the Earth's magnetic field is removed, the residual field is used to interpret the rocks. Rocks rich in magnetite, pyrrhotite, or illmenite have the most pronounced effects and generate the largest anomalies. Magnetic gradients near the edges of magnetic anomalies often indicate the location of faults or other boundaries.

Audiomagnetotelluric Soundings

AMT soundings (13 scalar and 25 tensor) were collected during the course of the study (fig. 1). Both types of soundings were used to provide depth-to-water estimates. The station names, locations, and estimates of depths to water in the regional aquifer are given in the section entitled "**Supplemental Data**" at the back of the report.

Natural-source AMT is an electromagnetic (EM) sounding technique in which the variation in resistivity of the ground as a function of depth is measured (Keller and Frischknecht, 1966). Soundings are obtained by measuring the magnitude of coherent signal peaks in the electric and magnetic fields. These peaks are generated by lightning and other atmospheric disturbances that provide a range of electromagnetic signals at various frequencies measurable at land surface. As an EM signal passes over a point on the Earth, a small amount of energy is transmitted vertically into the ground. The part of the EM signal that is transmitted attenuates exponentially with depth. The lower-frequency signals are less attenuated and penetrate farther than the higher-frequency signals. EM measurements made over a range of frequencies give information about resistivity variations with depth. EM measurements made at and below a frequency of 1 hertz are called magnetotelluric (MT). EM measurements made within the audio-frequency range are called AMT (typically 1 hertz to 30 kilohertz).

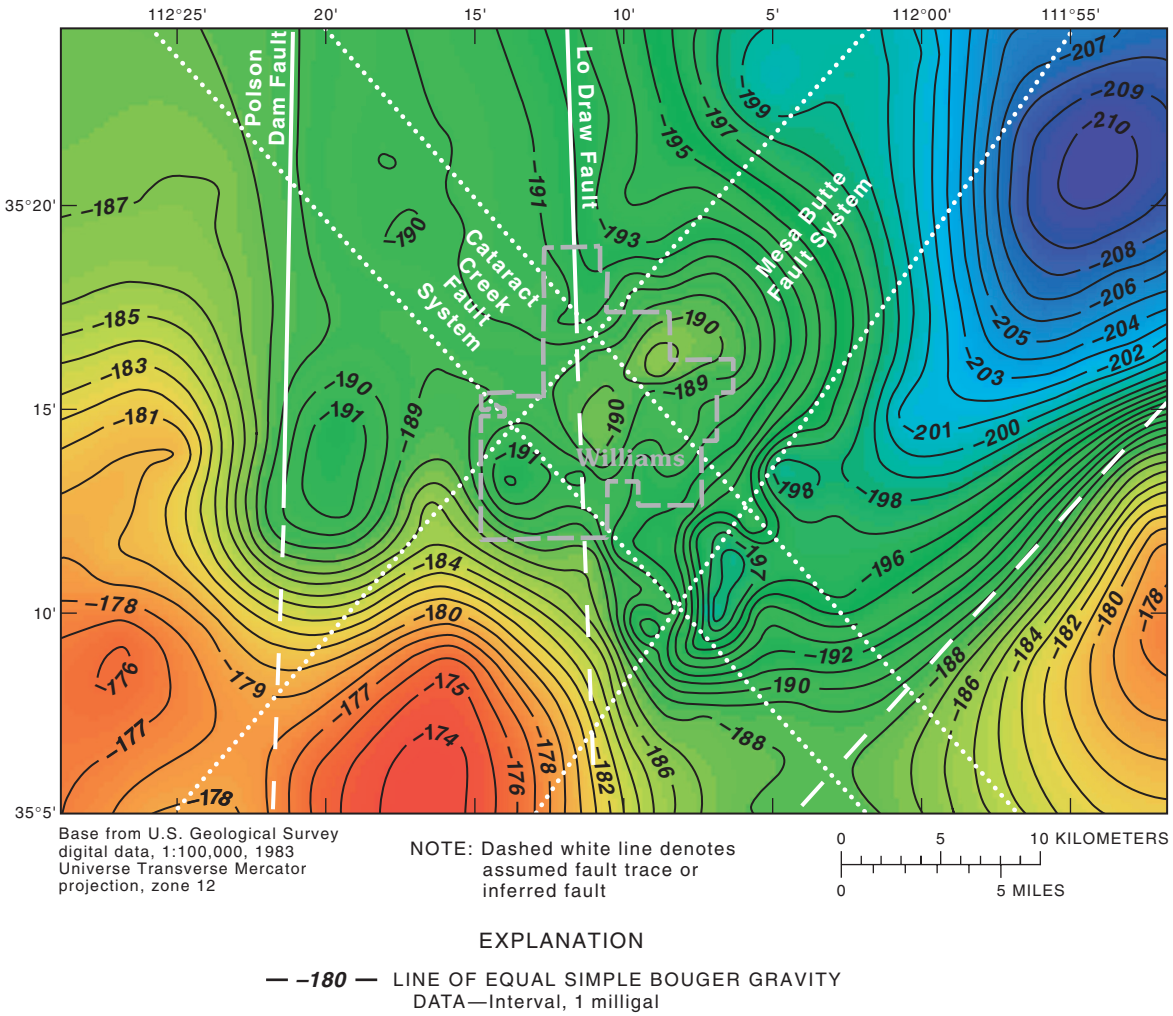

Figure 5. Simple Bouguer gravity anomaly map generated from the 2-kilometer grid of the U.S. Geological Survey and new gravity data near Williams, Arizona. Cooler colors are gravity lows; warmer colors are gravity highs. Fault identification and orientation based on gravity data.

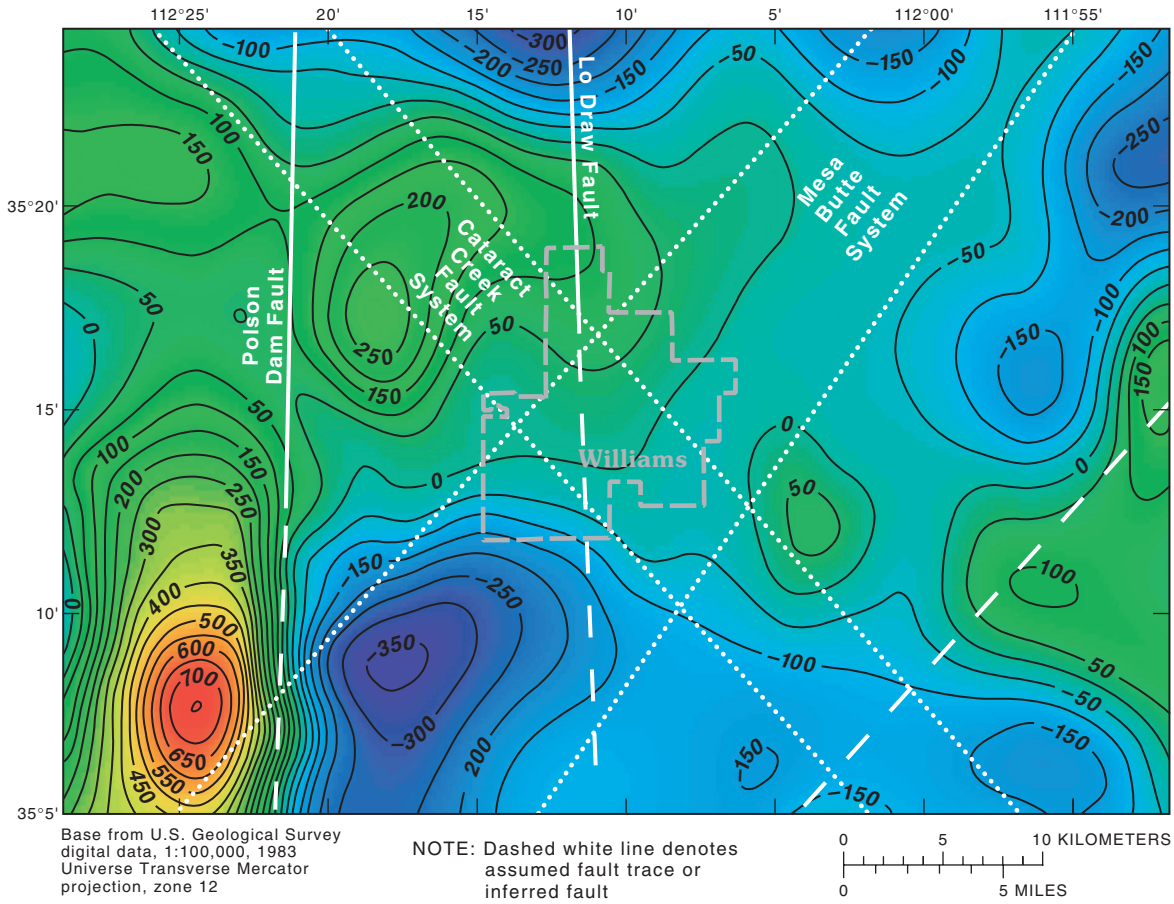

Figure 6. Aeromagnetic anomaly map generated from the 2-kilometer grid of the U.S. Geological Survey, Universal Transverse Mercator projection, near Williams, Arizona. Warmer colors represent magnetic highs; cooler colors represent magnetic lows. Fault identification and orientation based on aeromagnetic data.

Scalar AMT is a method in which one electric component (E_x) and one orthogonal magnetic component (H_y) are used to define the apparent resistivity (Sheriff, 1991). The vector electric field (E) in volts per meter and the vector current-density field (J) in amperes per square meter are related by the resistivity tensor (ρ_a) in which $E=\rho_a J$. If the material sampled is isotropic, then ρ_a is a scalar value. Scalar AMT is applicable to areas such as basins where isotropic horizontal layering can be assumed. The scalar AMT technique gives only an approximation of the true resistivity in areas with complex geology.

Cagniard (1953) discusses MT theory, interpretation, and potential applications and provides a formula for calculating Cagniard resistivity:

$$\rho_a = \left(\frac{0.2}{\nu}\right)\left(\frac{|E_x|}{|H_y|}\right)^2, \quad (1)$$

where

ρ_a = apparent resistance, in ohm-meters;
ν = frequency in hertz;
E_x = magnitude of the electric field in the x direction, in millivolts per kilometer; and
H_y = magnitude of the magnetic field in the y direction, in gammas.

Tensor AMT methods are better suited to areas with complex geology. The tensor method measures two orthogonal horizontal electric and magnetic fields. These fields are: E_x, electric field in the x direction; E_y, electric field in the y direction; H_x, magnetic field in the x direction; and H_y, magnetic field in the y direction. The impedance matrix (Z), therefore, can be described as a complex tensor to account for anisotropy and two-dimensional structures. The impedance is the apparent resistance, in ohms, to the flow of alternating current analogous to resistance in a direct-current circuit. Impedance is complex and of magnitude, Z, and has a phase angle, γ. These terms can be expressed in terms of resistance (R), inductive reactance ($X_L=2\pi\nu L$), and capacitive reactance ($X_C=1/2\pi\nu C$):

$$Z = [R^2 + (X_L - X_C)^2]^{1/2}, \quad (2)$$

where

R = resistance, in ohms;
L = inductance, in henrys;
C = capacitance, in farads; and

$$\gamma = \tan^{-1}[(X_L - X_C)^2]^{1/2}, \quad (3)$$

where

γ = phase angle, in radians.

In tensor AMT exploration, if E_x is the electric-field component in an arbitrary horizontal direction, and H_y is the associated orthogonal horizontal magnetic field, the surface impedance $Z_{surface}$ is:

$$Z_{surface} = E_x/H_y. \quad (4)$$

Measurements of surface impedance and frequency can be interpreted in terms of the electric properties of the subsurface. Vozoff (1986, 1991) discusses fundamental principles, data processing, analysis, noise, modeling, inversion, instrumentation, data acquisition, and case histories for the tensor-magnetotelluric method. The same techniques can be applied to the tensor-AMT method. The traditional technique for interpreting EM soundings is to find a model that closely reproduces the observed data (Spies and Frischknecht, 1991). Models can be found by curve matching, by interactive trial-and-error matching using a computer, or by automated computer programs. Techniques are available that use partial-curve matching or mathematical relations. The degree to which the physical model corresponds to the actual model depends on the type, completeness, and quality of the data, as well as on the geology.

Inverse-computer modeling allowed a starting layered-earth model to be adjusted to best fit the data. Ridge regression (Inman, 1975) was used to iteratively adjust the values of resistivity and thickness for the starting model using a least-squares fit. The starting layered-earth model can have as many as eight layers and can be constrained if some values of resistivity and thickness are known or can be estimated before inversion.

Smooth modeling also has been used to automatically interpret the MT amplitude and impedance-phase sounding data in terms of a smooth model. The model depths are spaced logarithmically and are generated from a minimum and maximum depth on the basis of a Bostik one-dimensional inversion or William of Occam's smooth inversion (Constable and others, 1987).

Estimated depth of exploration is a function of frequency (ν) and resistivity (ρ_a) and is approximated by the skin depth (δ) of the electromagnetic waves. The skin depth is the depth at which the fields have decreased to 37 percent (1/e) of their surface value and is:

$$\delta = \sqrt{\frac{\rho_a}{(\mu\pi\nu)}}, \qquad (5)$$

where

$\mu = \mu_0 =$ $4\pi \times 10^{-7}$, in weber per ampere meter.

Bostick (1977) provides for the calculation of depth (D_{meters}) to conductors. This one-dimensional inversion technique is given as:

$$D_{meters} = 355\sqrt{\left(\frac{\rho_a}{\nu}\right)}. \qquad (6)$$

Bosticks's equation gives a practical estimate of depth of exploration particularly if a well-defined descending branch (a conductor) is observed on a sounding curve. Because the Earth is being sampled laterally as well as vertically at the measuring station, simple one-dimensional model interpretations provide only an approximation of the true geoelectric section. If low-resistivity layers are encountered in the shallow subsurface, the curves may not reflect the true vertical-resistivity distribution because of signal attenuation and lateral effects caused by three-dimensional geologic structures.

Scalar-AMT sounding setup and data collection requires an electric dipole with nonpolarizing electrodes and an orthogonal magnetic sensor. Ten or more coherent electric and magnetic signals are digitized at each of 16 sampled frequencies (2.7, 4.5, 7.5, 14, 27, 45, 75… up to 14,000 hertz). The two-channel scalar AMT receiver used in this study used a 25-meter dipole and 1.3-meter magnetic coil. The scalar AMT receiver is a portable unit suitable for use in rugged terrain or in areas where vegetation prohibits the use of long lengths of wire. Cagniard (1953) resistivity values were calculated using appropriate instrument calibration and gain corrections (Long and Pierce, 1984). Application and details of the scalar AMT method are given by Strangway and others (1973). Hoover and others (1976, 1978) and Hoover and Long (1975) provide details about the USGS scalar AMT system used in this study.

Tensor AMT soundings require two electric dipoles with four nonpolarizing electrodes and two orthogonal-magnetic sensors (three if the vertical magnetic field, H_z, is measured). The tensor system used was a 10-channel receiver manufactured by Electromagnetic Instruments Incorporated (EMI, Berkeley, California). The EMI (MT-1) system collects coherent signals and calculates phase and impedance for as many as 60 equal log-spaced frequencies from 2.2 to 24,000 hertz. Scalar and tensor soundings (examples shown in **figures 7** and **8**) were modeled using the EMIXMT software by Interpex Limited (1993). Interpreted curves for each sounding were used to estimate depth to the water table.

Square-Array Resistivity

A recent study near Flagstaff, Arizona, included SAR and seismic-reflection work (Bills and others, 2000). The SAR provided a means to estimate fracture strike direction and depth to water. The high-resolution seismic-reflection profiles confirmed the SAR strike direction and the near-vertical nature of the faults on the Coconino Plateau. The fractures associated with faulting serve as pathways for ground-water flow and strongly influence the ground-water flow patterns near Flagstaff. On the basis of this experience, four SAR soundings were completed in the Williams area near Poquette Homestead, McDougal Flat, Williams Airport Road, and Bard Spring (**fig. 1**).

The SAR method is similar to that for traditional collinear arrays. The location of the array is the center of four electrodes that are laid out in a square pattern.

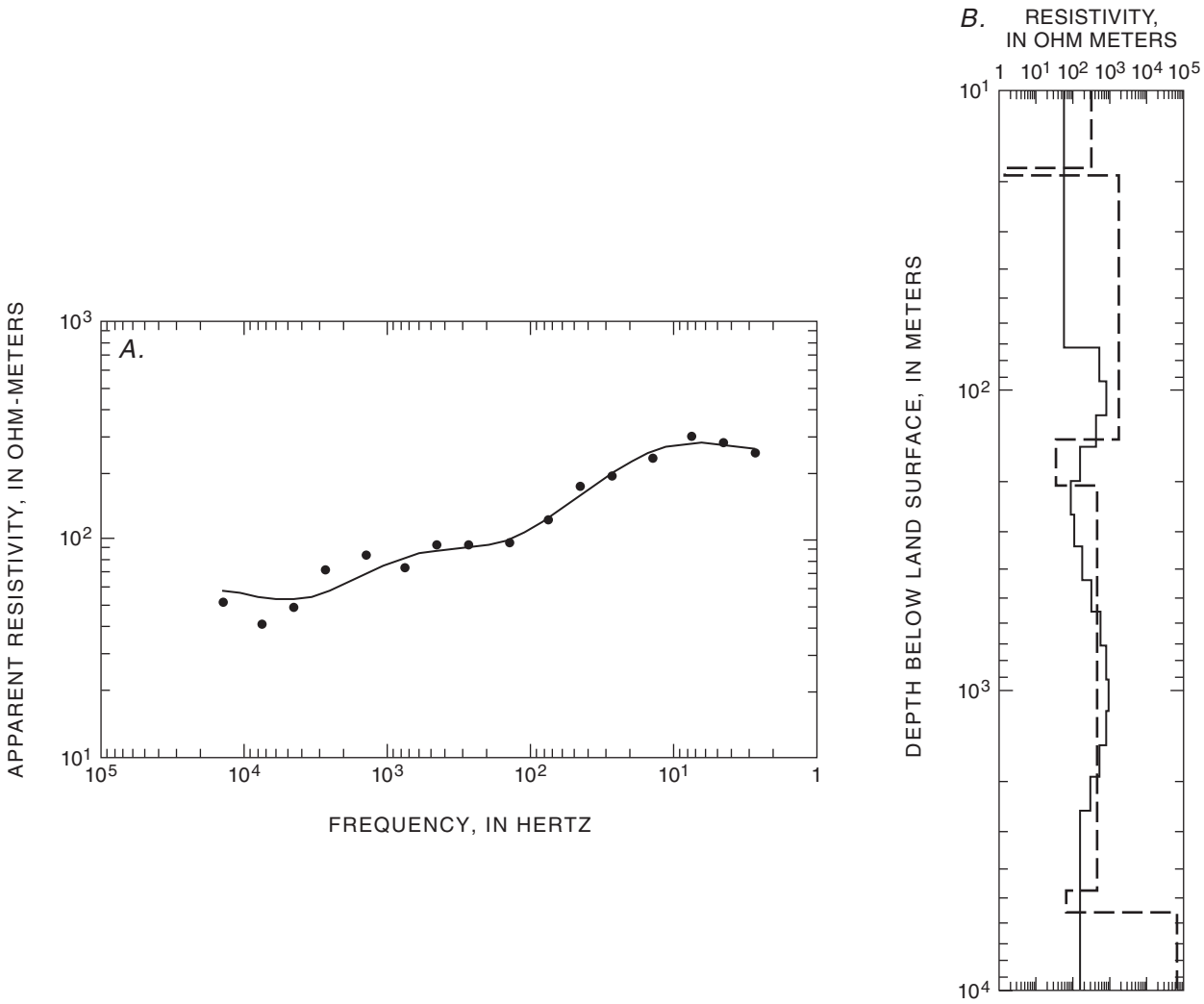

Figure 7. Scalar audiomagnetotelluric sounding data and model for data collected near the A-1 well site near Williams, Arizona. *A,* Scalar audiomagnetotelluric sounding data. *B,* Layered earth model (dashed line) and smooth model (solid line).

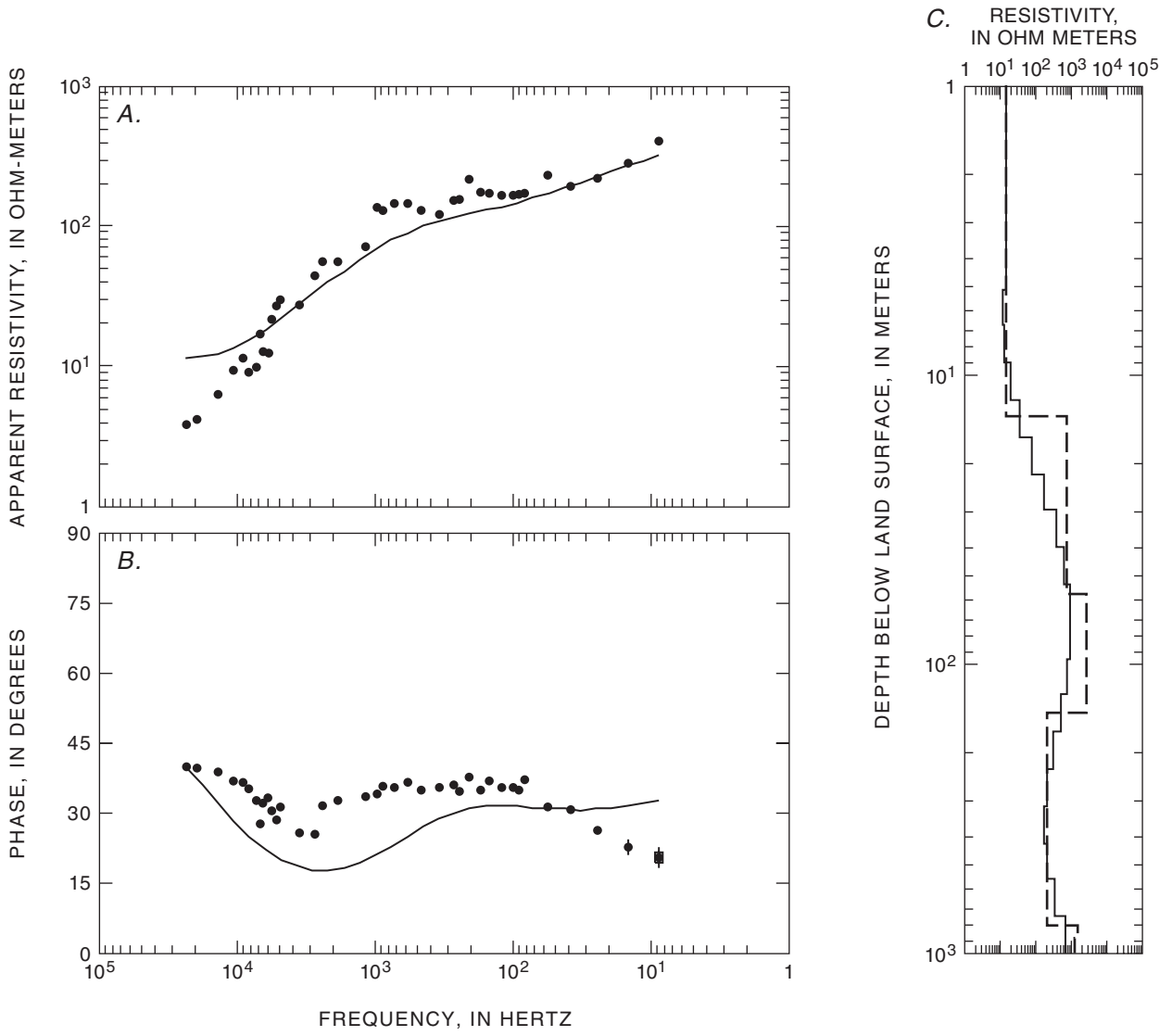

Figure 8. Tensor audiomagnetotelluric sounding data and model for data showing electric and magnetic field coherencies better than 0.8 recorded in Davenport Lake (dry) site (EMI-3) about 10 kilometers east of Williams, Arizona. *A*, Tensor audiomagnetotelluric sounding data. *B*, Phase audiomagnetotelluric sounding data. *C*, Layered earth model (dashed line) and smooth model (solid line).

The square size is equal to the length of one side of the square (A). Resistivity measurements are collected in three directions, two measurements in the two orthogonal directions along the sides of the square and one diagonal measurement collected as a check measurement. The array then is expanded by a factor of $A\sqrt{2}$ (Habberjam and Watkins, 1967) so that the sounding can be interpreted as a function of depth. Estimates of the depth of exploration in isotropic homogeneous material are roughly equal to the length of the side of the square (A). The square is expanded until the desired size is reached. The wire is reeled in, and the orientation of the square is rotated usually by 10 to 15°. The process is repeated until the data have been collected through 180°. In this study, a 15°-rotation increment was used, providing 12 orientations.

Apparent resistivity values are calculated using the equation:

$$\rho_a = K\Delta V/I, \tag{7}$$

where

ρ_a = apparent resistance, in ohm-meters;

K = calculated as $K = 2\pi A/(2-\sqrt{2})$ is the geometric-correction factor for the square (Habberjam and Watkins, 1967), and A is equal to one side of the square, in meters;

ΔV = potential difference, in volts; and

I = current, in amperes.

The 12 azimuthal soundings are averaged; the points are translated by a factor of 1.172 (Habberjam, 1979) to the right to generate a Schlumberger (1920) resistivity curve and are processed using ATO, which is a computer program developed by Zohdy and Bisdorf (1989). Several plots from SAR soundings collected in a study by Bills and others (2000) showed a resistivity maximum usually followed by a resistivity low. The measured depth to the water table usually equaled the resistivity high (rollover point) just before the resistivity low caused by the more conductive water-saturated rocks (Bills and others, 2000).

Resistivity data from SAR soundings are plotted for each square size (A) using polar coordinates after Taylor and Fleming (1988). The plots allow the investigator to visually pick the dominant fracture trend, which is normal to the major ellipse axis. Lane and others (1995) and Habberjam (1979) demonstrated that fracture direction, coefficient of anisotropy, and secondary porosity can be calculated from square-array soundings. Alternatively, a least-squares fit of an ellipse to the data can provide the ellipse maxima and minima necessary for the calculation of the coefficient of anisotropy and secondary porosity as follows:

$$\lambda = \sqrt{(\rho_y/\rho_x)}, \tag{8}$$

where

λ = coefficient of anisotropy.

λ can be calculated for the rock unit given by the ratio of major-axis resistivity to minor-axis resistivity and the true resistivity normal to joint direction. An azimuthal-resistivity survey provides the effective bulk-resistivity values parallel to the joint and (or) fracture strike (ρ_x) and normal to the joint and (or) fracture strike (ρ_y).

Lane and others (1995) modified Taylor and Fleming's (1988) equation for use with a square-array accounting for the geometric differences between the square and collinear arrays:

$$\phi = \frac{(3.41\times10^4)(N-1)(N^2-1)}{N^2C(\rho_{max}-\rho_{min})}, \tag{9}$$

where

ϕ = secondary porosity, in percent;

N = effective vertical anisotropy;

C = specific conductance of ground water in microsiemens per centimeter at 25°C;

ρ_{max} = maximum apparent resistivity, in ohm meters; and

ρ_{min} = minimum apparent resistivity, in ohm meters.

$$N = \sqrt{(1+(\lambda^2-1)\sin\alpha^2)}, \tag{10}$$

where

α = dip of the fractures, in degrees.

If the fractures are vertical, then $N=\lambda$. These formulas enable calculations of apparent resistivity for several directions; apparent fracture strike angle, θ (in degrees); coefficient of anisotropy; and secondary porosity for each crossed square-array set of apparent resistivity values at each square size. Properties obtained from these formulas are used to characterize aquifer conditions and ground-water flow.

Thematic-Mapper Data

A 3,108-km^2 area approximately centered on Williams was analyzed using Landsat TM data (fig. 9). The Landsat 5 TM satellite collects radiation in seven spectral bands. Bands 1, 2, and 3 record data in the blue, green, and red parts of the visible spectrum, respectively. Band 4 collects in the near infrared, and bands 5 and 7 in the middle infrared. Band 6 collects radiation in the thermal infrared. The data collected in bands 1–5 and band 7 have a ground resolution of 30 by 30 m; the data collected in band 6 have a ground resolution of 120 by 120 m. These data commonly are resampled to a nominal ground resolution of 28.5 by 28.5 m.

The Landsat TM data used in this analysis were acquired on May 10, 1993 (USGS EROS Data Center Scene ID numbers LT5037035009313010 and LT5037016009313010). These data were enhanced digitally to emphasize the geomorphic and (or) topographic expression of faults and other large surface fractures. This enhanced digital image was analyzed visually to identify and map continuous linear to curvilinear alignments of natural landscape features that indicate bedrock faults and other large surface fractures (Dr. J. Dohrenwend, consultant, Above and Beyond, Inc., written commun., 1998).

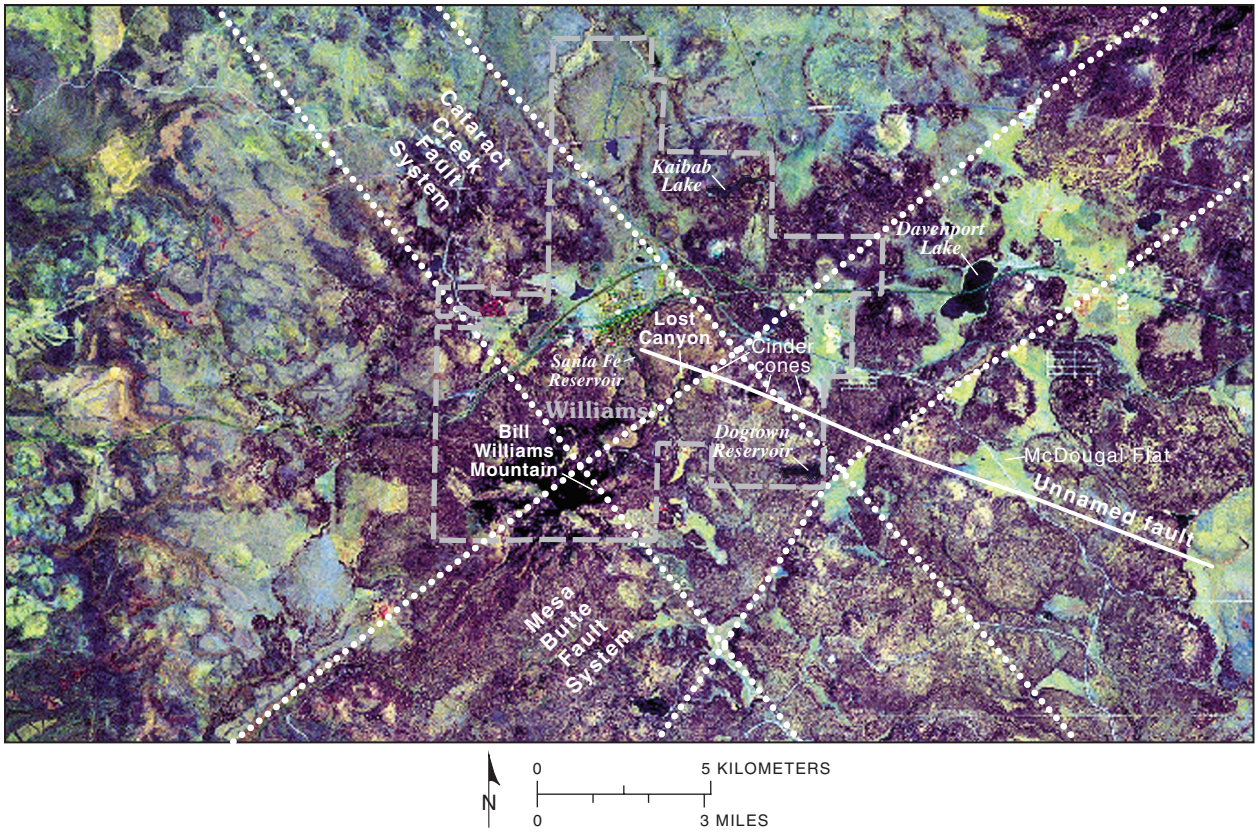

Figure 9. Landsat Thematic-Mapper image of the study area near Williams, Arizona. The northwestward-trending unnamed fault south and east of Williams was detected by square-array resistivity and audiomagnetotelluric soundings in McDougal Flat and intersects several cinder cones, Lost Canyon, and the Santa Fe Reservoir. Fault identification and orientation based on Thematic-Mapper data.

Aerial Photography

Photographs of an area of about 1,554 km^2 that extends north about 48 km and west about 32 km from Bill Williams Mountain were examined for indications of fracturing. Two sets of panchromatic, vertical, aerial photographs were used in the analysis: (1) National High Altitude Program (NHA) photographs that were taken in the summer and early fall of 1980 at an altitude of about 12,200 m (nominal scale of 1:80,000); and (2) National Aerial Photograph Program (NAPP) photographs that were taken in the summer of 1992 at an altitude of about 6,100 m (nominal scale of 1:40,000).

These aerial photographs were examined using a stereoscope with 3X binocular magnification. Such examination enables the resolution of features as small as 2 by 2 m on the 1:40,000-scale photographs. The resolution is 225 times smaller than the smallest features that can be resolved using the Landsat TM images. Linear to curvilinear alignments of natural landscape features that may indicate bedrock faults and other large surface fractures were identified and mapped using these photographs (Dr. J. Dohrenwend, consultant, Above and Beyond, Inc., written commun., 1998).

Digital Elevation Model Data

DEM is the terminology adopted by the USGS to describe terrain elevation data sets in a digital raster form. The 7.5-minute DEM provides coverage in 7.5- by 7.5-minute blocks. Resolution is 30- by 30-meter spacing on a UTM projection. The 7.5-minute DEM provides the same coverage as a standard USGS 7.5-minute quadrangle.

Many of the large structural features in the Williams area have a topographic signature. To assess these features, a DEM image for the area was compiled from four 7.5-minute USGS DEM quadrangles (**fig. 10**). The image covers 178 km^2.

Well Data

A total of 14 wells were located in the USGS ground-water site inventory (GWSI) database and the Arizona Department of Water Resources well-registry database. Seven of these wells are deep enough to yield water from the regional aquifer.

During the study, two wells near Williams were drilled, and lithologic sections were constructed from the drill cuttings. The A-1 well was drilled during 1995–96 by a private water company, and Bard Spring #2 well was drilled and logged in 1998 by the USGS Western Region drill rig. Lithologic information, geophysical logs, and depth-to-water data were used to provide ground truth for the geophysical-sounding methods.

HYDROGEOLOGIC UNITS

At the base of the hydrogeologic section are undifferentiated rocks of Precambrian age (**fig. 11**). Above the Precambrian rocks are consolidated sediments of Paleozoic age. These rocks extend over much of the Colorado Plateau Province (Fenneman, 1931). The geologic units include the Tapeats Sandstone, Bright Angel Shale, Muav Limestone, Temple Butte (Martin) Formation, Redwall Limestone, Supai Group, Hermit Formation, Schnebly Hill Formation, Coconino Sandstone, Toroweap Formation, and the Kaibab Formation. Saturated rocks include the Tapeats Sandstone, Bright Angel Shale, Muav Limestone, Redwall Limestone, and the bottom part of the Supai Group. Water quality in the Tapeats Sandstone and the Bright Angel Shale is too saline for most uses. A water sample from the Quivero well (1,123 m in depth) that is completed in the Tapeats Sandstone had a dissolved-solids concentration of 11,200 mg/L and a specific conductance of 18,000 µS/cm (Baroid, Inc., written commun., 1970). Water from the regional aquifer above the Tapeats Sandstone is used as drinking water in the communities of Valle and Tusayan, Arizona.

The regional aquifer in this study includes the Muav Limestone, the Redwall Limestone, and the base of the Supai Group. The total thickness of this sedimentary section varies but generally is about 1,100 m (Billingsley and others, 1980). Basaltic volcanic rocks of the San Francisco volcanic field mantel the entire study area.

Rocks of Precambrian age form the base of the hydrogeologic section. These rocks, where exposed in Grand Canyon, have low permeability and porosity and form the basal confining layer below the consolidated sediments.

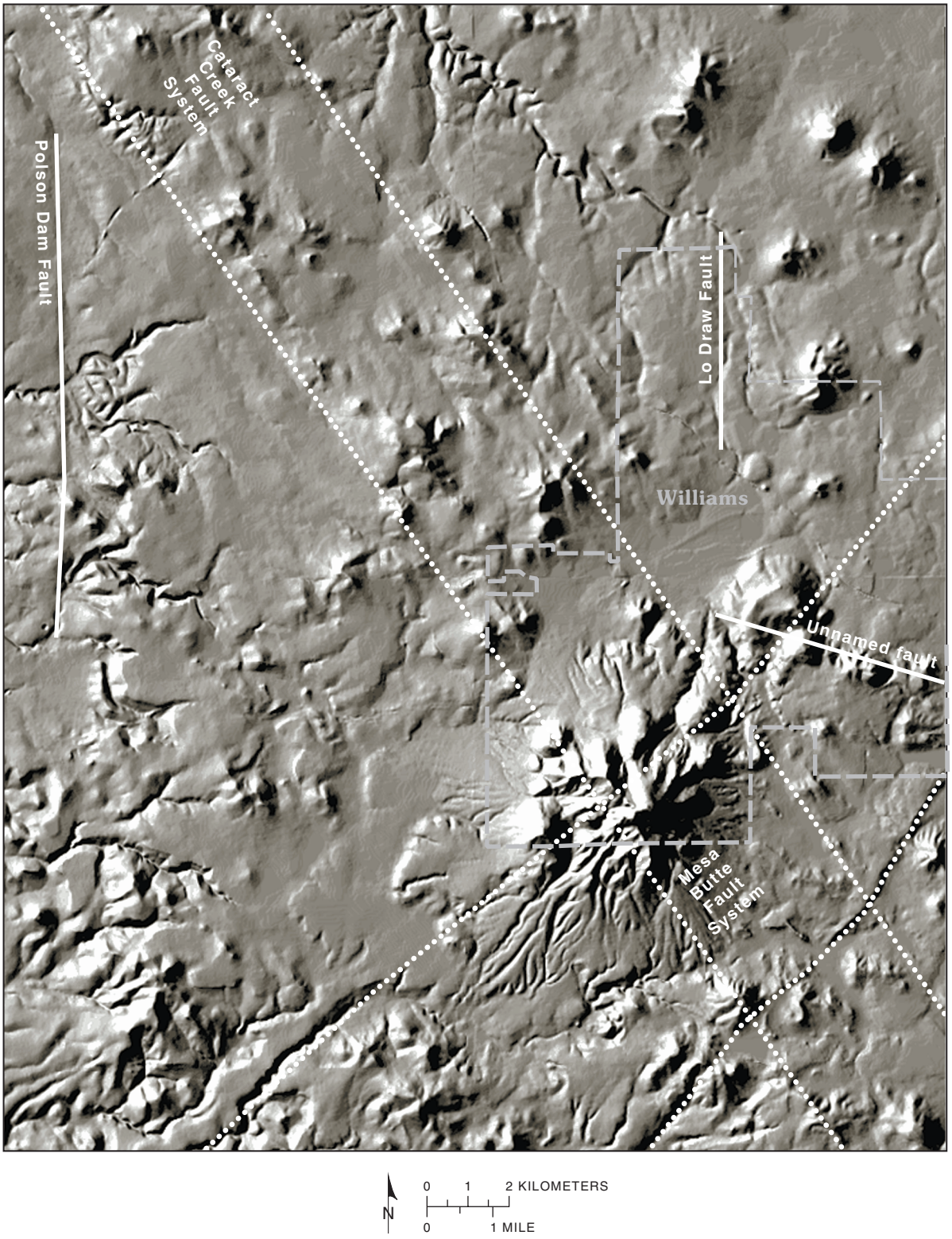

Figure 10. Mosaic of four 7.5-minute U.S. Geological Survey digital elevation models near Williams, Arizona. The unnamed fault in the eastern part of Williams was detected by square-array resistivity and audiomagnetotelluric soundings. Other faults were identified and oriented on the basis of digital elevation model data.

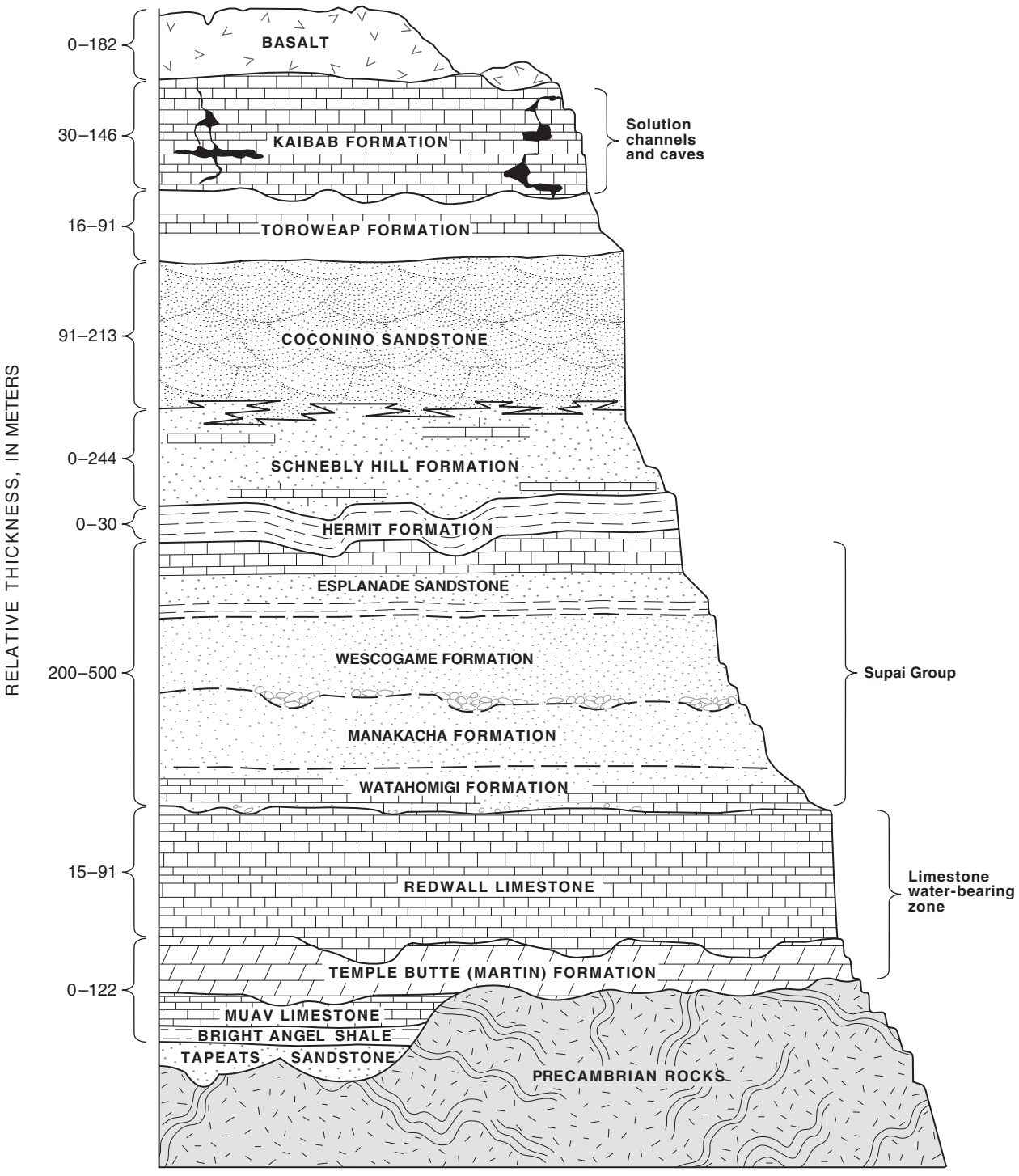

Figure 11. Rock formations and hydrogeologic units for the Williams area, Arizona.

The Tapeats Sandstone of Early Cambrian age is separated from the Precambrian rocks by an erosional unconformity (Hereford, 1975, 1977). The Tapeats Sandstone is the basal formation of the Tonto Group in the Grand Canyon area in Mohave and Coconino Counties, Arizona, and in the Colorado Plateau. The Tapeats Sandstone typically is between 53 and 55 m thick in the western part of Grand Canyon where the massive section is purple to buff, coarse-grained, thick-bedded, cross-laminated quartzite to quartzitic sandstone and the overlying transitional unit is a brown, coarse-grained, thin-bedded, ledge-forming, cream- to-brown quartzite or sandstone with some conglomerate beds and lenses near the base.

The Bright Angel Shale of Middle and Early Cambrian age is recognized as the middle formation of the Tonto Group within the Colorado Plateau (McKee, 1945). The fossiliferous shale is between the underlying Tapeats Sandstone and the overlying Muav Limestone and has gradational top and bottom contacts. The Bright Angel Shale is characterized by thin, platy laminations, green-buff color, glauconitic beds, and an abundance of worm markings. The Bright Angel Shale weathers to a slope or bench and ranges from 98 to 147 m in thickness in measured sections. Near Grand Canyon, the unit is green shale, platy, brown-spotted siltstone, and platy, micaceous, gray siltstone. This unit also may function as a basal or partial confining layer for the overlying regional aquifer near Williams.

The Muav Limestone, which is the upper formation of the Tonto Group, is Middle Cambrian in age. The formation is mapped on the north and south sides of the Colorado River and is recognized on cross sections and in measured sections from Mohave County to east of the Little Colorado River in the Colorado Plateau (McKee, 1945). The formation overlies and intertongues eastward with the Bright Angel Shale of the Tonto Group and unconformably underlies the Redwall Limestone. The section measures 139 m in thickness in Bass Canyon where the formation is composed of mottled-gray and buff, impure shaly and sandy limestone interbedded with fine-grained, buff sandstone. The formation forms steep slopes and cliffs and has coralloid and fucoidal markings but lacks fossils (Noble, 1914). The Muav Limestone is saturated and forms part of the regional aquifer near Williams.

The Temple Butte (Martin) Formation is Devonian in age (McNair, 1951; Teichert, 1968; Poole and others, 1967). In Arizona, this formation extends from the Basin and Range Province to the Black Mesa Basin and from the Colorado Plateau to the Pedregosa Basin. Poole and others (1967) have divided it into a lower unit, the Beckers Butte Sandstone Member of early Middle or possibly Early Devonian age, and an upper unit, the Jerome Member of Late Devonian age. The formation is light gray to dark gray. This formation also has been called the Martin Limestone or Martin Formation. Within the study area, it was not possible to distinguish this formation from the Redwall and Muav Limestones.

The Redwall Limestone of Mississippian and Pennsylvanian age unconformably overlies the Muav Limestone in Coconino County and in the Colorado Plateau (Noble, 1914; Armstrong and Holcomb, 1989). The Redwall Limestone is a dense, blue-gray crystalline limestone that forms a single cliff and underlies the Supai Group. This limestone ranges in thickness from 168 m on the trail near Grand Canyon station to 293 m east of Seligman, Arizona, on the east side of the Kaibab Plateau, and is 296 m thick in the Kanab Valley. Within the study area, the Redwall Limestone is saturated and forms part of the regional aquifer.

The Supai Group of Pennsylvanian to Permian age unconformably lies on the Redwall Limestone and similarly underlies the Hermit Formation. The group is a series of marine transgressional sediments deposited in an embayment of a Pennsylvanian sea. The group is recognized through most of the Arizona part of the Colorado Plateau, comprises four formations, and ranges in total thickness from about 200 to 530 m (McKee, 1982). The marine Watahomigi Formation, the lowest unit, is largely carbonate in composition and ranges from chert and flint gravels to fine-grained limestones. The Manakacha Formation overlies the Watahomigi Formation, grades from marine to continental from west to east, and is considerably sandier than the underlying Watahomigi Formation. The Wescogame Formation unconformably overlies the Manakacha Formation and, like the underlying unit, grades from marine to continental from west to east. This formation is sandier still than the Manakacha Formation and includes a basal conglomerate that partially fills erosional channels and depressions and blankets much of its depositional extent. The Permian Esplanade Sandstone overlies the Wescogame

Formation and is the thickest and most extensive part of the Supai Group. This shelf deposit ranges from thick-bedded limestones and sandstone in the west and east, respectively, that sit atop a basal mudstone or siltstone. In the A-1 well near Williams, the potentiometric surface is 2 m below the contact between the Supai Group and the Redwall Limestone.

A red shaly siltstone, the Hermit Shale, was deposited on an eroded, unconsolidated Supai surface (Noble, 1923). This formation was not observed in drill cuttings from wells in the Williams area.

The Schnebly Hill Formation of Early Permian age is named for exposures on the south side of Casner Canyon in Coconino County. The unit overlies the Supai Group in the Williams area and underlies the Coconino Sandstone at Fossil and Carrizo Creeks, at Fort Apache, and in the southern part of the Defiance Plateau. The formation includes sandstone, siltstone, mudstone, evaporites, and carbonates and ranges from 0 to 274 m in thickness. The unit is absent at Chino Point and at Grand Canyon, thickens toward the southeast, and is thickest (274 m) in the Holbrook Basin. The unit is present in the subsurface in wells east of Grand Canyon and is exposed on the Mogollon Rim, Mount Elden near Flagstaff, Defiance Plateau, and in some quarries north of Williams (Blakey, 1990). The Schnebly Hill Formation is unsaturated near Williams.

The Coconino Sandstone of Early Permian age extends across all of northern and central Arizona from the Defiance Plateau and the Monument Upwarp to northeastern Arizona. The lower part of the Schnebly Hill Formation intertongues with the Coconino Sandstone near Williams. The Coconino Sandstone is a cross-stratified, noncalcareous quartzarenite of eolian origin (Blakey, 1990). The unit ranges in thickness from 91 m at Bass Trail to 213 m in an escarpment 24 km southwest of Bill Williams Mountain (Darton, 1910). The formation is unsaturated near Williams.

The Toroweap Formation of Early Permian age overlies and intertongues with the Coconino Sandstone. The formation unconformably underlies the Kaibab Formation in the Sycamore Canyon-Sedona area in Yavapai County. The Toroweap Formation is recognized west of a line that runs from Sycamore Canyon north through Marble Canyon of Grand Canyon (Blakey, 1990). West of the study area near the Hurricane Cliffs in Mohave County, the Toroweap Formation is 131 m thick (Sorauf and Billingsley, 1991); and near Williams, the Toroweap Formation is 76 to 91 m thick (Bills and others, 2000). The formation is unsaturated.

The Kaibab Formation of early Permian age overlies the Toroweap Formation. The Kaibab is divided into the Fossil Mountain Member (base) and the Harrisburg Member (top) west of a north-south line in Arizona from Page in Coconino County in the Colorado Plateau to the Verde Valley and Prescott areas in Yavapai County in the Basin and Range Province. East of the north-south line, the formation consists of calcareous sandstone and sandstone and is not divided. The formation ranges from 30 to 250 m in thickness where it overlies the Toroweap Formation and unconformably underlies the Moenkopi Formation. The Fossil Mountain Member consists of fossiliferous limestone, white chert, and a yellow sandstone bed. The Harrisburg Member consists of interbedded limestone, gypsum, dolomite, chert, and sandstone, and has fossil brachiopods and gastropods. Total thickness for the Kaibab Formation near Williams is 146 m (Sorauf and Billingsley, 1991), and the formation generally is unsaturated although some small perched zones exist.

Newhall and others (1987) mapped and dated the basaltic rocks of Cenozoic age exposed in the Williams area. These basaltic flows cover an area of about 5,200 km^2 and vary in thickness from 0 to 300 m. Although andesitic, dacitic, and rhyolitic rocks also are found in the volcanic field, these rocks are concentrated in the larger volcanic centers (such as Bill Williams and Sitgreaves Mountains). The smaller, more numerous vents (mostly cinder cones) and associated flows are composed primarily of basalt, basaltic andesite, and benmoreite. These basalt flows typically are unsaturated although exceptions do exist. The truck stop at Beaumont, east of Williams on Interstate 40, has a productive well completed in basalt. Several springs near Bill Williams Mountain appear to be associated with brecciated flow bottoms, near-vertical joints, or faults. Springs on the flanks of Bill Williams Mountain are due to discontinuous fine-grained ash flows and tuffs that restrict the vertical flow of water locally.

Shallow alluvial wells in Pittman Valley and other topographically low areas yield water to ranches and homes. During extended periods of drought, the springs and the thin, discontinuous, and shallow aquifers have dried up because of pumping and infiltration.

Errol L. Montgomery and Associates, Inc. (1996) state that the Redwall-Muav aquifer is:

> *"...considered the only aquifer of regional extent that is capable of consistently yielding large quantities of groundwater to wells and springs..."*

They estimated that 98 percent of the water from this part of the Coconino Plateau discharges from the regional aquifer at Havasu Springs, which has a flow of 1,830 L/s. The remainder of the water discharges from smaller springs, usually at rates of less than 19 L/s, along the south rim of Grand Canyon.

STRUCTURAL CONTROLS ON GROUND-WATER CONDITIONS

The southwestern part of the Colorado Plateau has been affected by large-scale folds of Laramide age (Kelley, 1958; Chapin and Cather, 1981; Nations and others, 1985; and Davis and Kiven, 1975). The resulting large synclinal basins, anticlinal uplifts, and many smaller folds generally trend to the northwest in the study area and have been found in New Mexico and Utah (**fig. 2**). Examples of undulating basin uplift structures from west to east in northern Arizona are the Grand Canyon Embayment (a synclinal basin northwest of Bill Williams Mountain), the Kaibab Uplift, Black Mesa Basin, and the Defiance Uplift.

Within the study area, the synclinal Grand Canyon Embayment northwest of Bill Williams Mountain is the most important basin. The basin is bounded on the southeast by the Mesa Butte Fault system and on the east by the Kaibab Uplift. Two large fault systems cross the study area at right angles. The Mesa Butte Fault system trends northeast across the study area, and the Cataract Creek Fault system trends to the northwest (figs. 1, 5, 6, 9, and 10). These large throughgoing fault systems are as much as 14 km wide in some places and intersect near Bill Williams Mountain. The two fault systems are so pervasive that multiple subparallel fractures can be identified easily from gradients in the aeromagnetic and gravity data sets or from linear or curvilinear features on the TM and DEM images. Two smaller mapped faults, the Lo Draw and Polson Dam Faults, to the north and to the west, respectively, strike north and south (**fig. 10**).

These fault trends and other lineaments have been mapped using gravity (**fig. 5**), aeromagnetic (**fig. 6**), Landsat TM image (fig. 9), aerial photograph, DEM (fig. 10), and other surface-geophysical techniques. On a smaller scale, aerial photographs were used to identify or delineate north-south trending linear features on the west side of Bill Williams Mountain near Bard Spring before the Bard Spring #2 well was drilled.

The gravity map (fig. 5) shows a 10 Mgal low in the northeastern part of the study area. The northeastward- and southwestward-trending gravity low is bounded by the Mesa Butte Fault system on the northwest, the Cataract Creek Fault system on the southwest, and an unmapped feature on the southeast that probably is a fault. This gravity low is thought to be a fault-bounded graben or small subbasin filled with volcanic rock.

The aeromagnetic map (fig. 6) shows the Mesa Butte and Cataract Creek Fault systems. These fault systems, the Polson Dam Fault and an unnamed fault, are closely associated with the locations of magnetic gradients. On the basis of interpretation of aeromagnetic data, Shoemaker and others (1978) suggest that as much as 8 km of right lateral offset can be inferred from the basement-aeromagnetic anomalies.

The enhanced digital TM image (**fig. 9**) was analyzed visually to identify and map continuous linear to curvilinear alignments of natural landscape features that indicate bedrock faults and other large surface fractures. The large fault systems have been mapped on the image to show locations.

DEMs (fig. 10) show the two north-south trending faults, Polson Dam and Lo Draw, mapped by Newhall and others (1987) and one unnamed fault interpreted from the SAR and AMT sounding data. The image shows surface traces of the two major fault systems as they cut through Bill Williams Mountain. Several other subparallel fractures associated with the northwestward-trending Cataract Creek Fault system and the northeastward-trending Mesa Butte Fault system can be seen on figure 10.

The highly fractured and block-faulted rocks limit the occurrence and extent of shallow perched aquifers. The fault blocks, though nearly horizontal, usually are in contact with near-vertical, throughgoing and active faults that may provide vertical flow paths to the regional aquifer. The near-vertical (<10°) nature of the faults has been imaged on seismic-reflection profiles by Catchings and others (1997) west of the study area in Flagstaff, Arizona.

INTERPRETED DEPTH TO GROUND WATER IN THE REGIONAL AQUIFER

Wells in the study area.—Only seven wells near the study area are completed in the regional aquifer (fig. 1; table 1); one of these wells is bridged, and one well yields water of poor quality for most uses. Only the 1,067-meter-deep A-1 well (table 1) is completed in the Redwall and Muav Limestones in Williams. The Gonzalez and the Klinke wells were drilled into the graben on the Cataract Creek Fault system in Williams (table 2). These two dry, 762-meter-deep wells were completed in the Supai Group. Four wells along State Highway 64 to the north toward Grand Canyon are completed in the regional aquifer. The Quivero well is 29 km north of Interstate 40 along State Highway 64 near the intersection of the highway and the Black Mesa Pipeline. As of 1999, the community of Valle has three wells. The Valle 1 well is 549 m deep and yields water from a perched zone above the regional aquifer. East of Williams along Interstate 40, the Santa Fe well (near the Klinke well) is completed in the regional aquifer, and the community of Ash Fork has two wells that are completed in the regional aquifer. Measured depth-to-water data from these wells were used in conjunction with interpreted sounding estimates for the water-table interpretation.

The A-1 well is bridged at about 884 m below land surface and above the water table in the Redwall Limestone. Before bridging occurred, the driller indicated that water could be air lifted at a rate of about 9.5 L/s. A lithologic log was compiled from cuttings collected every 6.1 m (Bradley Baum and D.J. Bills, hydrologists, USGS, written commun., 1998). This well provided lithologic information and a local depth to water in the regional aquifer (**fig. 12**). In addition, a video log was completed to 150 m before large solution caverns and unstable rock in the Kaibab Formation halted the work. An unexpected observation from the A-1 well cuttings was halite crystals in the Supai Group. Although no halite was observed in wells near Flagstaff, Aiken and Sumner (1972) noted halite in the evaporites of the upper part of the Supai Group near Holbrook, Arizona.

Table 1. Data for selected wells that discharge water from the regional aquifer near Williams, Arizona

[Minus signs on longitude values indicate west longitude]

Well name	Latitude	Longitude	Water-level altitude, in meters	Date water level measured
Quivero	35°31'34"	-112°09'49"	1,014	12–16–1969
Valle 2	35°39'20"	-112°08'25"	1,068	12–28–1994
Valle 3	35°39'29"	-112°07'50"	1,050	6–15–1994
Santa Fe (near Klinke well)	35°15'46"	-112°25'26"	1,058	10–1–1931
A-1 well	35°14'56"	-112°07'28"	[1]1,178	3–1997
Ash Fork 1	35°12'49"	-112°28'37"	1,248	1–1988
Ash Fork 2	35°12'07"	-112°28'37"	1,254	10–17–1997

[1]Altitude at which water was first encountered during drilling. Hole later collapsed.

Table 2. Dry wells near Williams, Arizona

[Minus signs on longitude values indicate west longitude]

Location	Latitude	Longitude	Altitude of the bottom of hole, in meters	Year drilled
Santa Fe #1	35°19'24"	-112°21'18"	1,186	1952
El Paso Gas	35°18'19"	-112°03'30"	1,357	1978
Klinke well	35°14'44"	-112°27'58"	1,250	1941
Gonzalez well	35°15'29"	-112°11'51"	1,291	1963
Bard Spring #2	35°12'16"	-112°16'07"	1,621	1998
Santa Fe #3	35°15'13"	-112°10'49"	1,762	1960

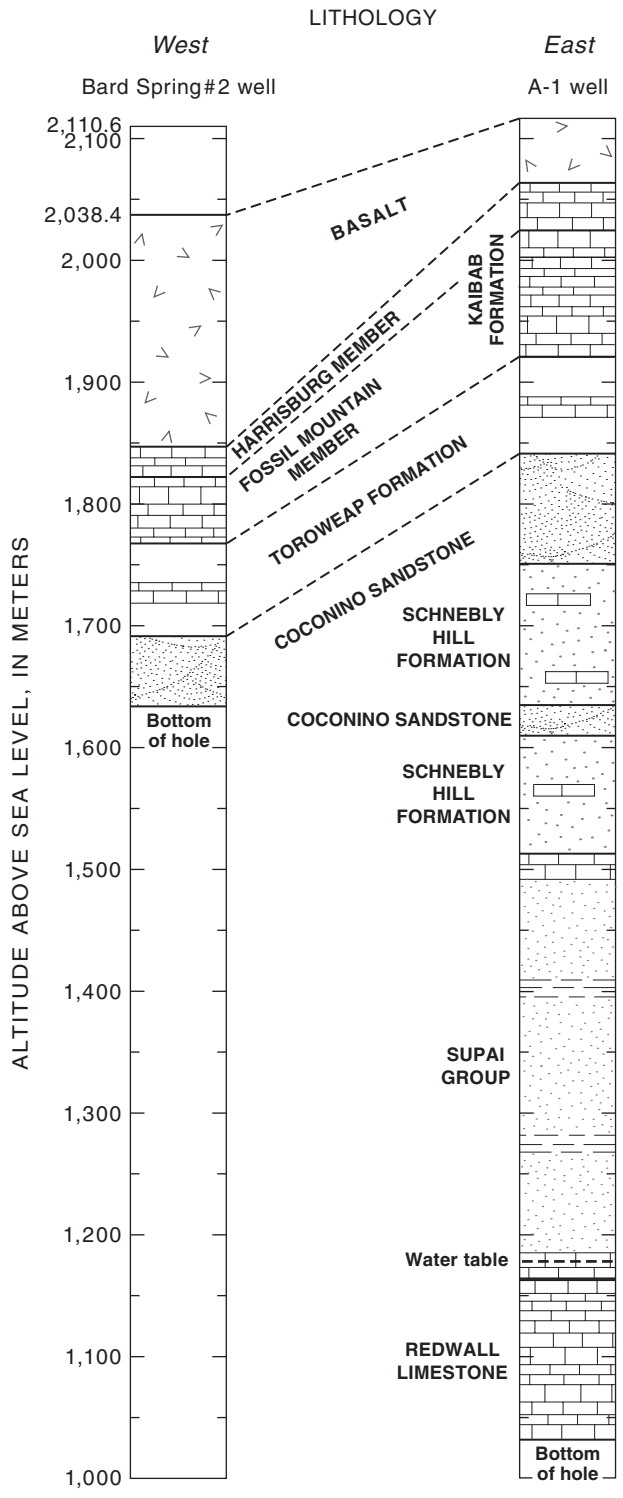

Figure 12. Lithologic logs derived from well cuttings analyzed every 6.1 meters in two wells near Williams, Arizona. Bard Spring #2 well is 4.82 kilometers west of Bill Williams Mountain near Pine Springs, and A-1 well is 8 kilometers east of the city of Williams along Interstate 40. Water table is at an altitude of 1,178 meters above sea level.

Data from geophysical surveys in the Bard Spring area indicate perched ground-water conditions in a small basin west of Bill Williams Mountain. An exploration hole was drilled in 1998 near Bard Spring to test the observations and provide stratigraphic and borehole-geophysical information. The Bard Spring #2 well is 401 m deep and did not reach the regional aquifer. A lithologic log (fig. 12) was compiled from cuttings taken every 3.0 m (Bradley Baum and D.J. Bills, hydrologists, USGS, written commun., 1998). In May 1998, induction-borehole-conductivity logs were collected and show that the basalt has a mean conductivity of 140 μS/m (standard deviation of 36.7 μS/m). The Kaibab Formation below the basalts has a mean conductivity of 3.9 μS/m (standard deviation of 0.64 μS/m). The Toroweap Formation has slightly higher and more variable conductivity values and a mean of 8.6 μS/m (standard deviation of 5.6 μS/m). The Coconino Sandstone has a mean conductivity of 3.8 μS/m (standard deviation of 0.3 μS/m). The high conductivity values in the basalts may be caused by water or altered zeolites. Two video logs recorded on May 14, 1998, and on July 24, 1998, show moisture on the basalt in the well bore from near the end of the casing at 46 m below land surface to 200 m below land surface. The accumulated moisture on the well bore does not provide any usable flow, and the formations below the basalt are dry (**fig. 13**).

An estimated depth-to-water map and an estimated water-table map were compiled using data from several sources. Measured water levels from wells completed in the regional aquifer were augmented with SAR-derived depth-to-water estimates and with AMT depth-to-water estimates from layered-earth models (**figs. 14** and **15**). The SAR estimates are based on interpreted curves derived from a computer program (ATO) developed by Zohdy and Bisdorf (1989). The AMT depth-to-water estimates are based on layered-earth models generated from the apparent resistivity values and sampled frequencies. The general direction of water flow is to the northwest from Bill Williams Mountain toward the Cataract Creek Fault system and the main northern discharge point at Havasu Springs. The apparent ground-water gradient between A-1 well in Williams and the Valle wells is -0.003 to the north.

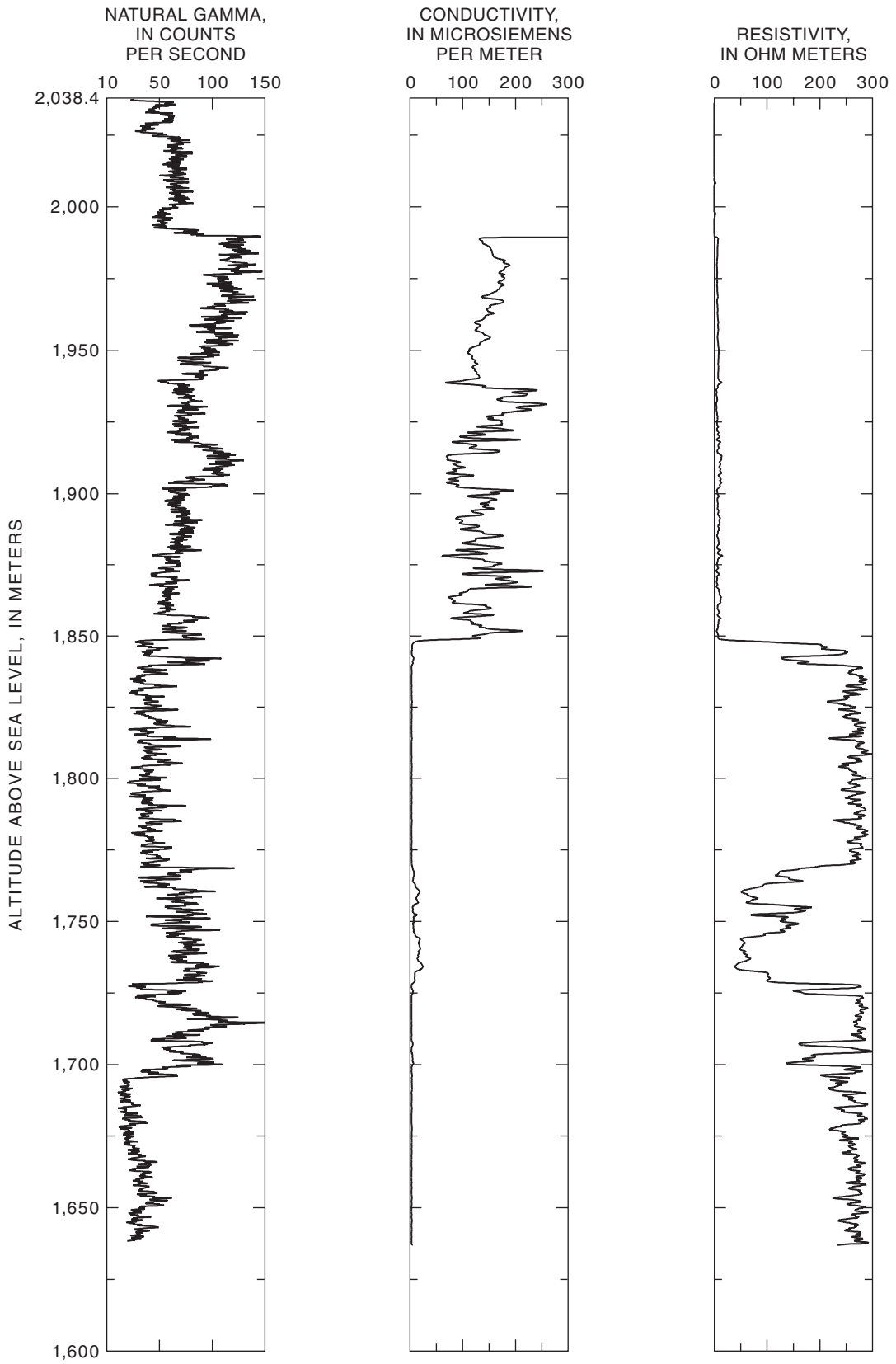

Figure 13. Geophysical logs and lithology for Bard Spring #2 well, Williams, Arizona. The borehole data include natural gamma, conductivity, resistivity, caliper, and two temperature logs.

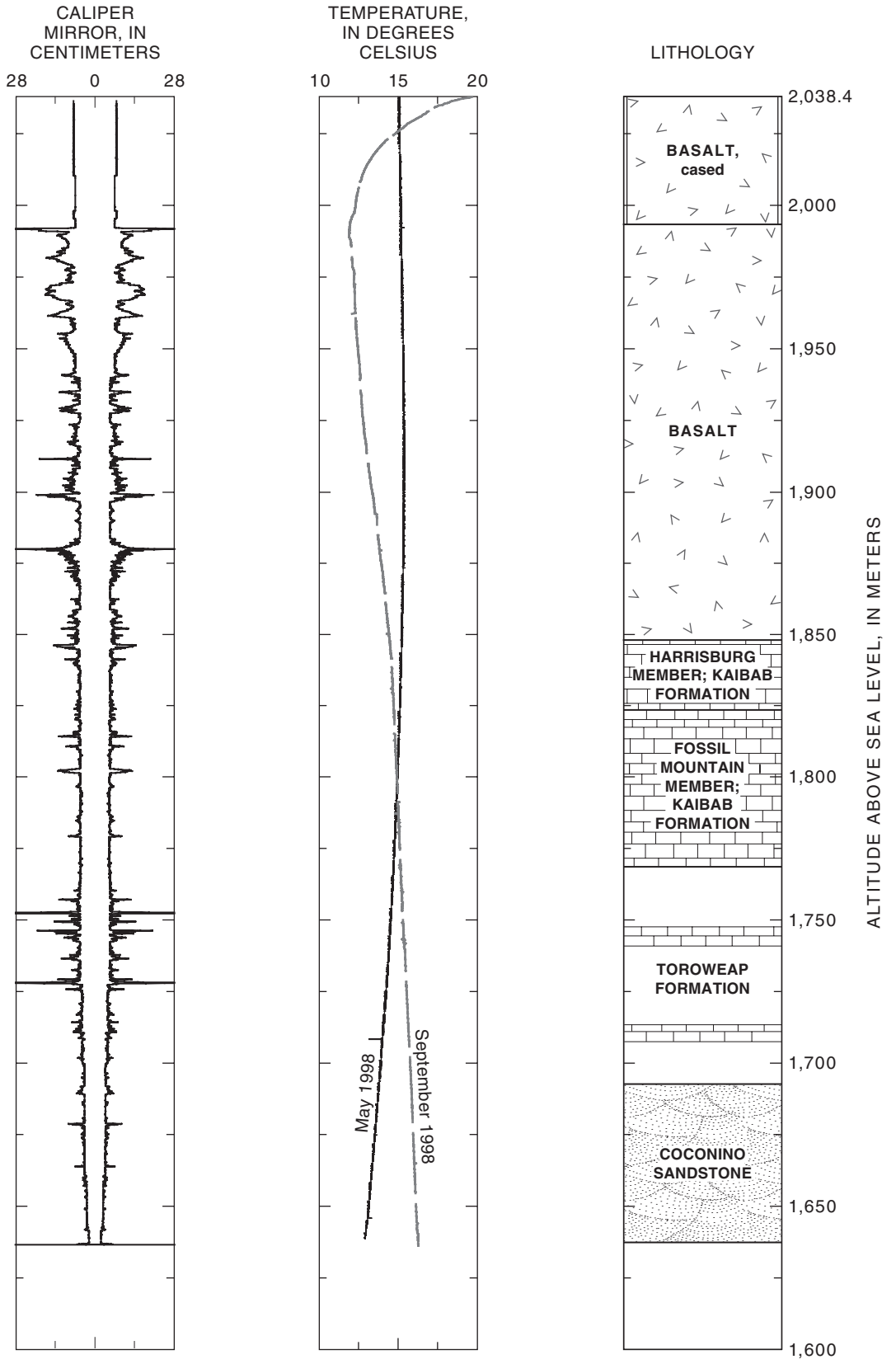

Figure 13. Continued.

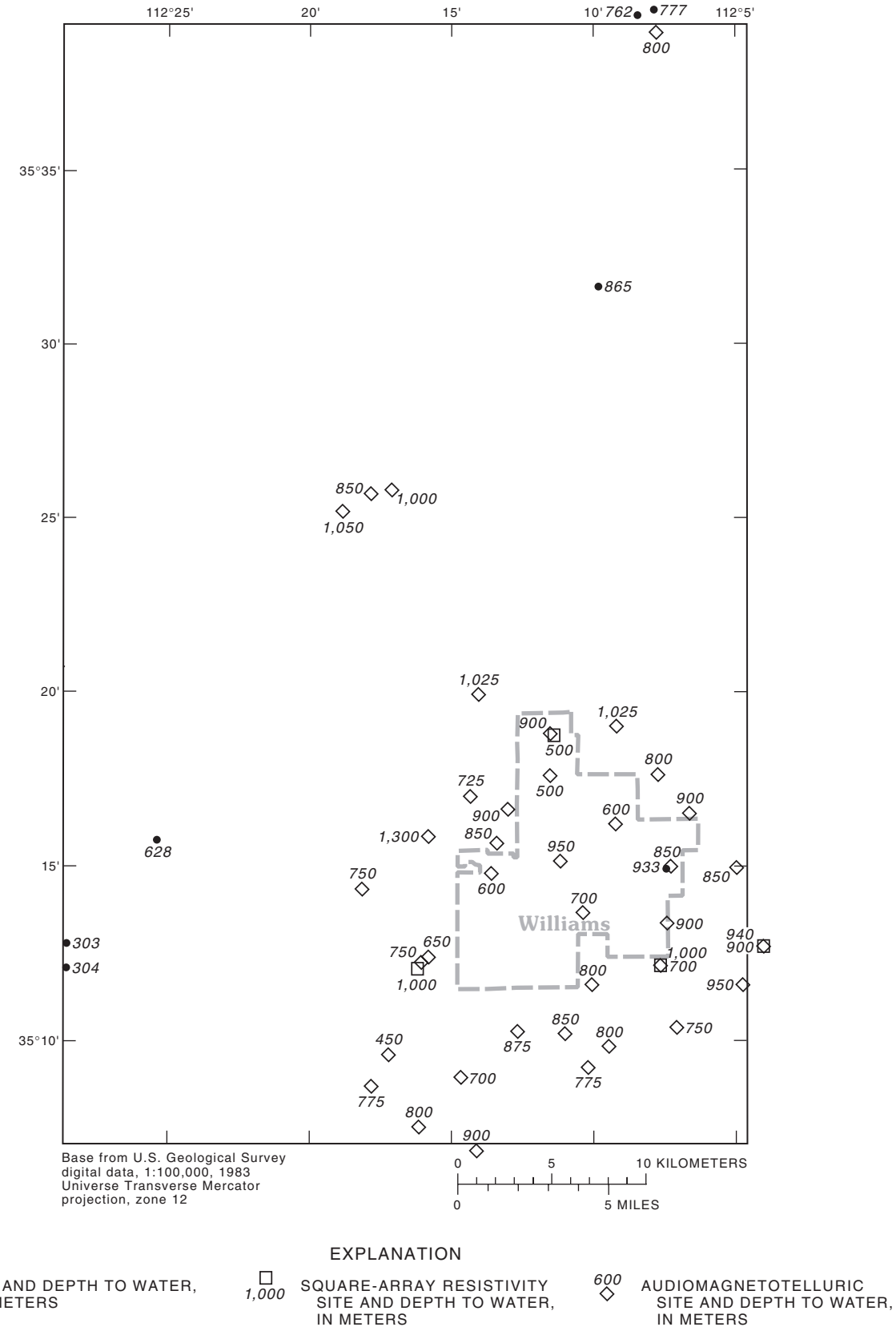

Figure 14. Depth to water, Williams, Arizona. No altitude corrections have been applied. Data are from 7 wells, 4 square-array resistivity soundings, 25 tensor audiomagnetotelluric soundings, and 11 scalar audiomagnetotelluric soundings.

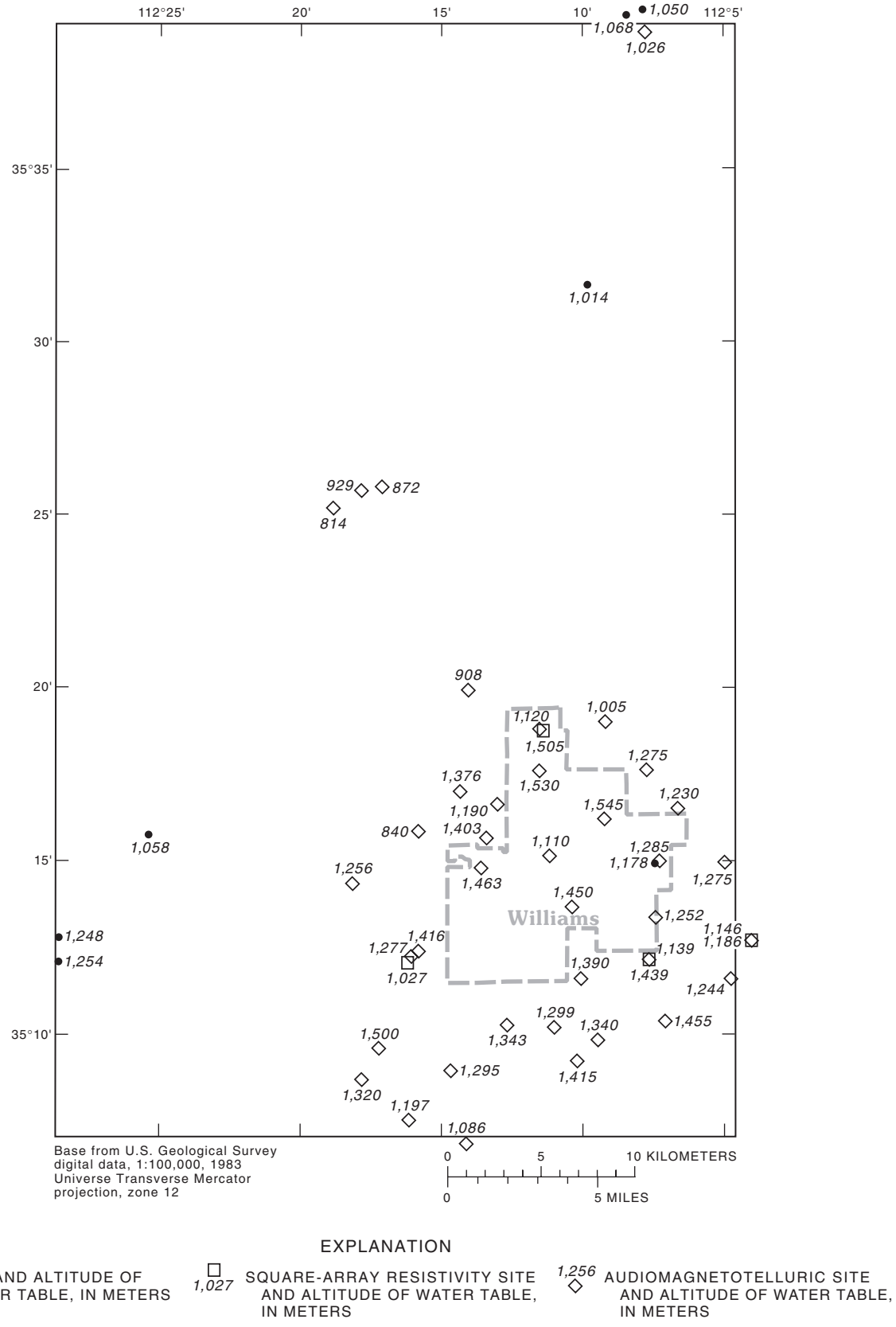

Figure 15. Altitude of the water table, Williams, Arizona. Data are from 7 wells, 4 square-array soundings, 25 tensor audiomagnetotelluric soundings, and 11 scalar audiomagnetotelluric soundings.

Estimated Aquifer Properties

Secondary porosity values estimated from the four SAR soundings varied from 0.1 to 9.6 percent. The coefficient-of-anisotropy values ranged from 1.01 to 1.34. SAR mean resistivity, coefficient of anisotropy, secondary porosity, and fracture-strike azimuth were plotted against depth for each of the four sites (figs. 16–19).

The 980-meter-deep SAR sounding at the Williams Airport Road site has a mean resistivity curve that gradually increases with depth from about 140 Ω•m near the surface to more than 500 Ω•m at depth (**fig. 16**). The coefficient of anisotropy, secondary porosity, and strike azimuth can be divided into an upper half and a lower half for the sounding. The upper 500 m of the sounding has the largest coefficient of anisotropy (1.3 for the 0- to 40-meter-depth range) and the highest secondary porosity (7 percent). A value of 1.04 over the lower 500 m of the sounding indicates little fracturing and secondary porosity of generally less than 0.5 percent at this site.The upper 500 m of the sounding has fracture strikes that are almost due east. Below 500 m, the fracture-strike direction is predominately to the northwest. The northwestward trend calculated from the SAR data is in line with the Cataract Creek Fault system.

The mean resistivity curve for the SAR sounding at the Bard Spring site increases rapidly from 150 Ω•m near the surface to 300 Ω•m at a depth of 50 m (**fig. 17**). Resistivity gradually decreases to about 110 Ω•m at a depth of 300 m. The decrease probably is due to the moisture content in the basalts and the fine-grained volcanic material as observed in the Bard Spring #2 well. The coefficient of anisotropy averages about 1.1 from 0 to 350 m, which indicates abundant fracturing. The ratio then drops to 1.04 from 500 to 850 m. At 1,000 m, the coefficient of anisotropy has a small peak at 1.08. Secondary porosity follows the coefficient of anisotropy pattern of high-low-high. Secondary porosity reaches a high of 2.5 percent in the 0- to 350-meter range, drops to less than 1 percent for the 500- to 850-meter range, and then recovers to 1 percent at 1,000 m. The strike direction gradually changes from due north at the surface to northwest at a depth of 650 m. At 850 m, the strike direction is rotated due north again and is rotated back to the northwest at 1,150 m.

The mean resistivity curve for the SAR sounding at McDougal Flat increases from 28 Ω•m near the surface to about 400 Ω•m near a depth of 1,300 m, which indicates a smoothly increasing electrical section (**fig. 18**). The coefficient-of-anisotropy ratio increases from near unity at the surface to 1.12 at a depth of 350 m. The ratio then remains near 1.12 to a depth of 1,300 m. Secondary porosity is near zero at the surface, near 4 percent at 125 m, then gradually tapers down to about 1 percent at a depth of 1,300 m. The strike direction for this sounding is northwest from 0 to 200 m and then predominantly N. 60° W. from 500 to 1,300 m. The strike direction matches an unnamed fault and a line of cinder cones that trend northwestward to the Santa Fe Reservoir. Analysis of aerial photography also indicates a lineament that trends in this direction.

The mean resistivity curve for the SAR sounding at Poquette Homestead increases from 40 Ω•m at the surface to about 600 Ω•m near a depth of 1,150 m, which indicates a resistive electrical section (**fig. 19**). The coefficient-of-anisotropy ratio is 1.0 at 50 m, increases to 1.22 at 350 m, and then is constant until 1,000 m. At 1,000 m, the ratio increases to 1.34, which is the highest measured in the Williams area. Secondary porosity is 9.5 percent near the surface, but at a depth of 50 m, the secondary porosity is near zero. The secondary porosity increases to near 2 percent for the 150- to 1,150-meter depth range. The strike direction swings from due east at the surface to due north by the 100-meter depth, then swings back to the northeast in the 250- to 1,150-meter depth range, and follows the trend of the Mesa Butte Fault system.

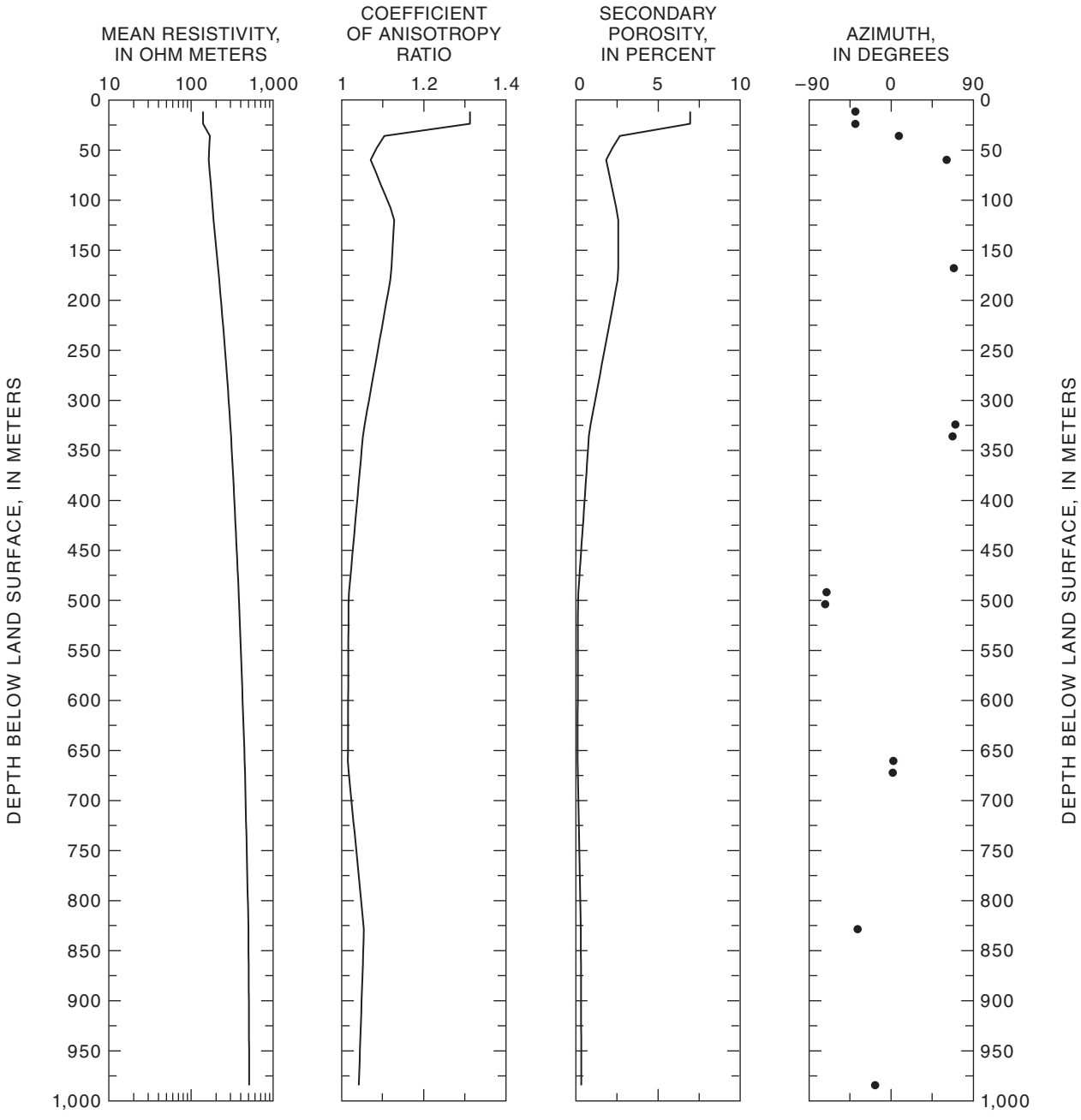

Figure 16. Square-array resistivity sounding data and estimated aquifer properties from the site at Airport Road, Williams, Arizona.

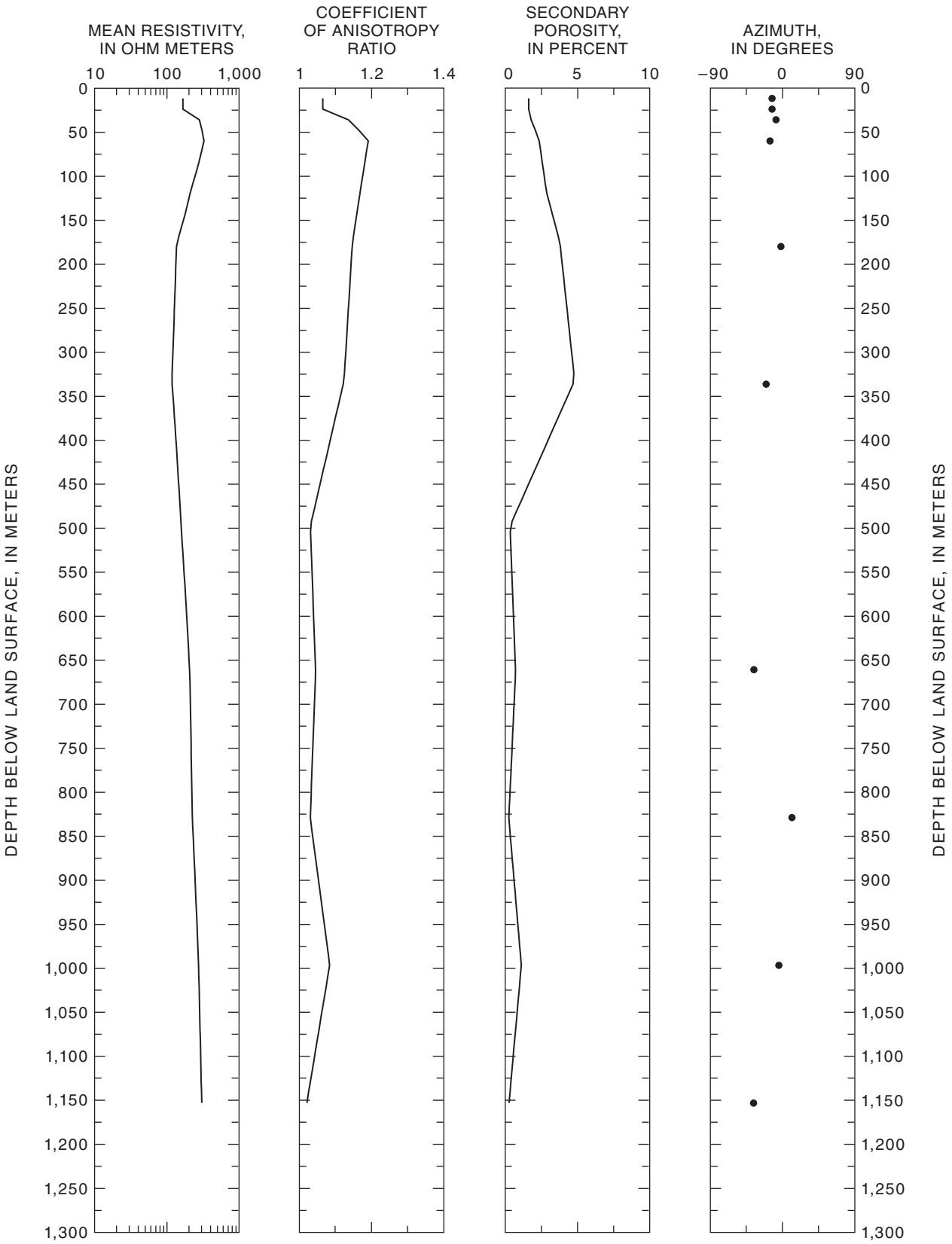

Figure 17. Square-array resistivity sounding data and estimated aquifer properties from the site at Bard Spring, Williams, Arizona.

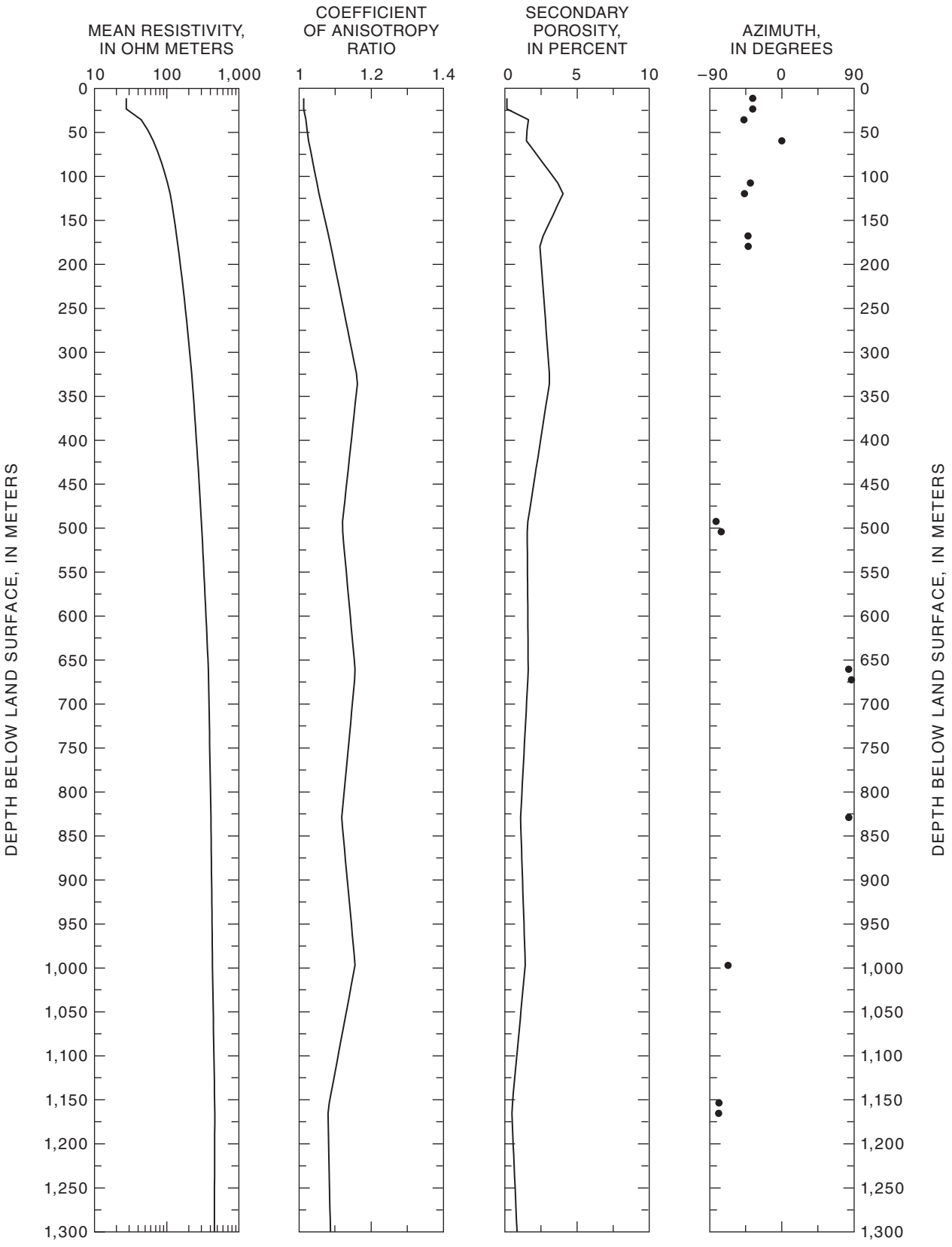

Figure 18. Square-array resistivity sounding data and estimated aquifer properties from the site at McDougal Flat, Williams, Arizona.

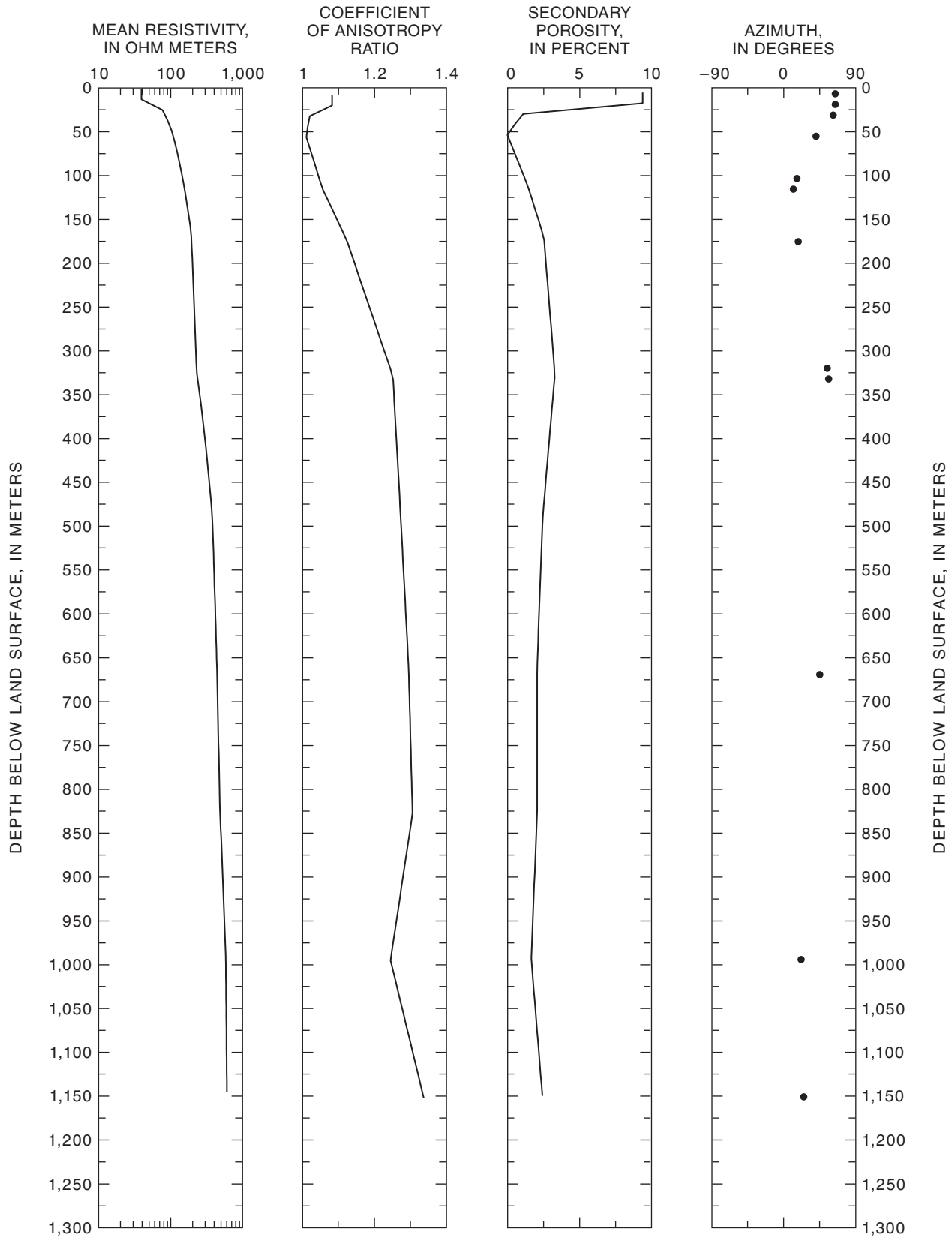

Figure 19. Square-array resistivity sounding data and estimated aquifer properties from the site at Poquette Homestead, Williams, Arizona.

SUMMARY AND CONCLUSIONS

In the area near Bill Williams Mountain, the volcanic and sedimentary rocks are cut pervasively by near-vertical, laterally continuous, and active normal faults. Most of these faults trend N. 45° W. and N. 45° E.; however, some faults trend north and south and at least one fault trends N. 60° W. These faults are evident in the magnetic, gravity, TM, and DEM images. The faults have broken the near-horizontal consolidated sediments that restrict the vertical movement of water to the regional aquifer. The active faults probably improve the vertical-hydraulic conductivity by providing many open near-vertical conduits to the regional aquifer. Below the regional water table, the near-vertical faults in the Redwall and Muav Limestones provide lateral flow to the discharge points. The lateral flow may be enhanced by solution features along fractures in the limestone aquifers.

Estimated depth to water in the regional aquifer varies with location on the basis of interpreted AMT and SAR sounding curves and few well data. Estimated depth to water ranges from 450 to about 1,300 m. Estimated altitudes of the water table range from about 814 to 1,545 m above sea level.

The coefficient of anisotropy calculated from the four SAR soundings ranged from 1.01 to 1.34. The highest coefficient-of-anisotropy value is at the bottom of the sounding for Poquette Homestead. Secondary porosity values estimated from the SAR soundings varied from 0.1 to 9.6 percent. The highest secondary porosity calculated at the surface of the sounding at Poquette Homestead is associated with fractured volcanic rocks. Mean resistivity from the SAR soundings varied from less than 30 Ω•m to more than 600 Ω•m. Strike direction depends on proximity to major structures. For example, the N. 45° E. trend was expected for the fractures at Poquette Homestead because the sounding was within 1 km of the 24-meter Mesa Butte Fault scarp near Dogtown Reservoir. The northwestward trend at McDougal Flat was unexpected. A previously unmapped fault that trends N. 60° W. was detected first by the AMT and SAR soundings then confirmed or verified on aerial photographs and DEM images by cinder-cone alignment. The northward-trending strike direction measured at the SAR site at Bard Spring coincides with the Polson Dam Fault north of Interstate 40. The N. 45° W. trend in the lower 500 m of the sounding at the site at Airport Road was due to the northwestward-trending Cataract Creek Fault system.

Because much of the data derived in this study were from surface techniques rather than well information, the inferred water levels should be viewed strictly as estimates. Additional wells in the area would provide data that could strengthen the limited control of the existing well data. Continued collection of well data as it becomes available is essential to add to the understanding of the hydrology of this part of the Coconino Plateau. Because of potential water-quality issues associated with the halite in the Supai Group and high dissolved solids in the lower part of the regional aquifer, the following approaches for further study of the area in and around Bill Williams Mountain may need to be considered in order to provide information to evaluate the ground-water quality in the area.

1. Continue to collect lithologic data from wells completed in the regional aquifer to refine the stratigraphic interpretations.
2. Determine the chemistry of well water collected from wells completed in the various formations along State Highway 64 north to Grand Canyon.
3. Describe the chemistry of water for all discharge points in the study area.
4. Estimate the age of water in the regional aquifer to improve the present understanding of recharge and ground-water flow paths.
5. Estimate the age of water from the volcanic springs and seeps to determine residence time in volcanic rocks of Tertiary and Quaternary age.

SELECTED REFERENCES

Aiken, C.L.V., and Sumner, J.S., 1972, A study of regional geophysical data in the Holbrook area, Arizona: Arizona Geological Survey Publication OG–23, 42 p. [Formerly published as Oil and Gas Conservation Commission Report of Investigations RI–2].

Armstrong, A.K., and Holcomb, L.D., 1989, Stratigraphy, facies and paleotectonic history of Mississippian rocks in the San Juan Basin of northwestern New Mexico and adjacent areas, *in* Evolution of sedimentary basins, San Juan Basin: U.S. Geological Survey Bulletin 1808–D, p. D1–D21.

Bills, D.J., Truini, Margot, Flynn, M.E., Pierce, H.A., Catchings, R.D., and Rymer, M.J., 2000, Hydrogeology of the regional aquifer near Flagstaff, Arizona, 1994–97: U.S. Geological Survey Water-Resources Investigations Report 00–4122, 143 p.

Billingsley, G.H., and Huntoon, P.W., 1983, Geologic map of the western Grand Canyon Formation, Arizona: Grand Canyon, Arizona, Grand Canyon Natural History Association map sheet.

Billingsley, G.H., Barnes, C.W., and Ulrich, G.E., 1985, Geologic map of the Coconino Point and Grandview Point quadrangles, Coconino County, Arizona: U.S. Geological Survey Miscellaneous Investigations Map I–1644, 1 sheet, scale, 1:62,500.

Billingsley, G.H., Breed, W.J., and Beasley, D., 1980, Geologic cross section along Interstate 40–Kingman to Flagstaff, Arizona: Chandler, Arizona, Pagosa Press, Petrified Forest Museum Association in cooperation with the Museum of Northern Arizona, map sheet.

Blakey, R.C., 1979, Stratigraphy of the Supai Group (Pennsylvanian-Permian), Mogollon Rim, Arizona, *in* Beus, S.S., and Rawson, R.R., eds., Carboniferous stratigraphy in the Grand Canyon Country, northern Arizona and southern Nevada: Falls Church, Virginia, American Geological Institute Guidebook Series No. 2, Ninth International Congress of Carboniferous Stratigraphy and Geology, p. 89–104.

____1990, Stratigraphy and geologic history of Pennsylvanian and Permian rocks, Mogollon Rim region, central Arizona and vicinity: Geological Society of America Bulletin, v. 102, no. 9, p. 1189–1217.

Blakey, R.C., and Knepp, R., 1989, Pennsylvanian and Permian geology of Arizona, *in* Jenney, J.P., and Reynolds, S.J., eds., Geologic Evolution of Arizona: Arizona Geological Society Digest 17, p. 313–347.

Bostick, F.X., Jr., 1977, A simple and almost exact method of MT analysis: Salt Lake City, University of Utah, Geothermal Workshop Report, p. 175–177.

Breed, W.J., Huntoon, P.W., and Billingsley, G.H., 1986, Geologic map of the eastern part of the Grand Canyon National Park, Arizona: Grand Canyon, Arizona, Grand Canyon Natural History Association, map sheet, scale 1:62,500.

Cagniard, Louis, 1953, Basic theory of the magnetotelluric method of geophysical prospecting: Geophysics, v. 18, no. 3, p. 605–635.

Catchings, R.D., Jaasma, M.N., Goldman, M.R., and Rymer, M.J., 1997, Seismic images beneath the Continental (Bottomless Pits) area of Flagstaff, Arizona: U.S. Geological Survey Open-File Report 97–76, 29 p.

Chapin, C.E., and Cather, S.M., 1981, Eocene tectonics and sedimentation in the Colorado Plateau-Rocky Mountain area, *in* Dickinson, W.R., and Payne, W.D., eds., Relations of tectonics to ore deposits in the southern Cordillera: Tucson, Arizona Geological Society Digest, v. 14, March 19–20, 1981 Meeting, Tucson, Arizona, p. 173–198.

Constable, S.C., Parker, R.L., and Constable, C.G., 1987, Occam's inversion—A practical algorithm for generating smooth models from electromagnetic sounding data: Geophysics, v. 52, no. 3, p. 289–300.

Damon, P.E., Shafiqullah, Mohammed, and Leventhal, J.S., 1974, K-Ar chronology for the San Francisco volcanic field and rate of erosion of the Little Colorado River, *in* Karlstom, T.N.V., Swann, G.A., and Eastwood, R.L., eds., Part 1 of Geology of Northern Arizona: Geological Society of America Guidebook for Rocky Mountain Section Meeting, Flagstaff, Arizona, v. 6, no. 5, p. 221–235.

Darton, N.H., 1910, A reconnaissance of parts of northwestern New Mexico and northern Arizona: U.S. Geological Survey Bulletin 435, 88 p.

Davis, G.H., and Kiven, C.W., 1975, Tectonic analysis of folds in the Colorado Plateau of Arizona: Tucson, University of Arizona, Office of Arid Lands Studies Bulletin 9, 68 p.

Doe, T.W., Long, J.C.S., Endo, H.K., and Wilson, C.R., 1982, Approaches to evaluating the permeability and porosity of fractured rock masses, *in* Goodman, R.E., and Hueze, F.E., eds., Issues in Rock Mechanics: New York, American Institute of Mining, Metallurgical and Petroleum Engineers, Inc., Proceedings of the Twenty-Third Symposium on Rock Mechanics, Berkeley, California, August 25–27, 1982, p. 30–38.

Fenneman, N.M., 1931, Physiography of western United States: New York, McGraw-Hill, 534 p.

Fetter, C.W., 1980, Applied hydrogeology: Columbus, Ohio, Charles E. Merrill Publishing Company, 488 p.

Habberjam, G.M., 1972, The effects of anisotropy in square-array resistivity measurements: Geophysical Prospecting, v. 20, no. 2, p. 249–266.

____1979, Apparent resistivity observations and the use of square-array techniques: Berlin, Germany, Bebruder Borntraeger, Geoexploration Monograph Series 1, no. 9, 152 p.

Habberjam, G.M., and Watkins, G.E., 1967, The use of a square configuration in resistivity prospecting: Geophysical Prospecting, v. 15, no. 3, p. 445–467.

Hereford, Richard, 1975, Chino Valley Formation (Cambrian?) in northwestern Arizona: Geological Society of America Bulletin, v. 86, no. 5, p. 677–682.

____1977, Deposition of the Tapeats Sandstone (Cambrian) in central Arizona: Geological Society of America Bulletin, v. 88, no. 2, p. 199–211.

Hoover, D.B., and Long, C.L., 1975, Audio-magnetotelluric methods in reconnaissance geothermal exploration [abs.]: Proceedings of the Second United Nations Symposium for the Development of Geothermal Resources, San Francisco, California, May 20–29, 1975, p. 1059–1064.

Hoover, D.B., Frischknecht, F.C., and Tippens, C., 1976, Audio-magnetotelluric soundings as a reconnaissance exploration technique in Long Valley, California: Washington, D.C., American, Geophysical Union, Journal of Geophysical Research, v. 81, no. 5, p. 801–809.

Hoover, D.B., Long, C.L., and Senterfit, R.M., 1978, Some results from audio-magnetotelluric investigations in geothermal areas: Geophysics, v. 43, no. 7, p. 1501–1514.

Huntoon, P.W., and Billingsley, G.H., 1981, Geologic map of the Hurricane Fault zone and vicinity, western Grand Canyon, Arizona: Grand Canyon Arizona, Grand Canyon Natural History Association, map sheet.

Inman, J.R., 1975, Resistivity inversion with ridge regression: Geophysics, v. 40, no. 5, p. 798–817.

Interpex, Inc., 1993, EMIX MT, v. 2.0, Magnetotelluric data interpretation software: Golden, Colorado, Interpex Limited.

Keller, G.V., and Frischknecht, F.C., 1966, Electrical methods in geophysical prospecting: London, Great Britain, Pergamon Press, 519 p.

Kelley, V.C., 1958, Tectonics of the Black Mesa Basin region of Arizona, *in* Anderson, R.Y., and Harshbarger, J.W., eds., 9th Field Conference Guidebook of the Black Mesa Basin, northeastern Arizona: New Mexico Geological Society, p. 146–150.

Lane, J.W., Jr., Haeni, F.P., and Watson, W.M., 1995, Use of a square-array direct-current resistivity method to detect fractures in crystalline bedrock in New Hampshire: Groundwater, v. 33, no. 3, p. 476–485.

Long, Carl, and Pierce, H.A., 1986, BASIC program to reduce audio-magnetotelluric data and calculate apparent resistivity: U.S. Geological Survey Open-File Report 86–200, 17 p.

Loughlin, W.D., and Huntoon, P.W., 1983, Compilation of available ground-water quality data for sources with the Grand Canyon of Arizona: U.S. National Park Service, unpublished report prepared under contract PX8210Z0883.

McKee, E.D., 1938, The environment and history of the Toroweap and Kaibab Formations of northern Arizona and southern Utah: Washington, D.C., Carnegie Institution of Washington Publication 492, 268 p.

____1945, Stratigraphy and ecology of the Grand Canyon Cambrian, Part 1—Cambrian history of the Grand Canyon region: Carnegie Institution of Washington Publication No. 563, p. 1–170.

____1954, Stratigraphy and history of the Moenkopi Formation of Triassic age: Geological Society of America Memoir 61, 133 p.

____1982, The Supai Group of the Grand Canyon: U.S. Geological Survey Professional Paper 1173, 504 p.

McNair, A.H., 1951, Paleozoic stratigraphy of part of northwestern Arizona: American Association of Petroleum Geologists Bulletin, v. 35, no. 3, p. 503–541.

Metzger, D.G., 1961, Geology in relation to availability of water along the south rim Grand Canyon National Park, Arizona: U.S. Geological Survey Water-Supply Paper 1475–C, p. 105–138.

Milsom, John, 1989, Field geophysics, *in* Cox, Keith, ed., Geological Society of London Handbook: New York, John Wiley & Sons, 181 p.

Montgomery, Errol, L., and Associates, Inc., 1996, Assessment of hydrogeologic conditions and potential effects of proposed groundwater withdrawal for Canyon Forest Village, Coconino County, Arizona: Tucson, Arizona, E.L. Montgomery and Associates, Inc., 64 p.

National Climatic Data Center, 2000, NCDC climate data online: U.S. Department of Commerce, National Oceanic and Atmospheric Administration, National Climatic Data Center, URL, http://cdo.ncdc.noaa.gov/plclimprod, accessed June 2000.

____1996, Climatological data annual summaries, Arizona: U.S. Department of Commerce, National Oceanic and Atmospheric Administration, National Climatic Data Center, v. 100, no. 13.

____1997, Climatological data annual summaries, Arizona: U.S. Department of Commerce, National Oceanic and Atmospheric Administration, National Climatic Data Center, v. 101, no. 13.

____1998, Climatological data annual summaries, Arizona: U.S. Department of Commerce, National Climatic Data Center, v. 102, no. 13.

Nations, J.D., Wilt, J.C., and Hevly, R.H., 1985, Cenozoic paleogeography of Arizona, *in* Flores, R.M., and Caplan, S.S., eds., Cenozoic Paleogeography of the West-Central United States, Rocky Mountain Paleogeography Symposium 3: Society of Economic Paleotologists and Mineralogists, p. 201–224.

Newhall, C.G., Ulrich, G.E., and Wolfe, E.W., 1987, Geologic map of the southwest part of the San Francisco volcanic field, north-central Arizona: U.S. Geological Survey Miscellaneous Field-Studies Map MF–1958, scale, 1:50,000, 58 p.

Noble, L.F., 1914, The Shinumo quadrangle, Grand Canyon district, Arizona: U.S. Geological Survey Bulletin 549, 100 p.

____1923, A section of the Paleozoic Formations of the Grand Canyon at the Bass Trail, in Shorter contributions to General Geology, 1922: U.S. Geological Survey Professional Paper 131–B, p. B23–B73.

Phillips, J.D., Duval, J.S., and Ambrosiak, R.A., 1993, National geophysical data grids—Gamma-ray, magnetic, and topographic data for the conterminous United States: U.S. Geological Survey Digital Data Series DDS-9, 1 CD-ROM.

Poole, F.G., Baars, D.L., Drewes, Harald, Hayes, P.T., Ketner, K.B., McKee, E.D., and Teichert, Curt, 1967, Devonian of the southwestern United States, *in* Oswald, D.H., ed.: Alberta Society of Petroleum Geologists, International Symposium on the Devonian System, v. 1, Calgary, Alberta, Canada, p. 879–912.

Ragozin, E.I., 1903, The use of electricity in investigations of ore bodies: St. Petersburg, Russia, I. Goldberg, s. 4, 442 p.

Schlumberger, Conrad, 1920, Essais de prospection électrique du sous-sol: Académie Science Comptes Rendus, v. 170, no. 9, p. 519–521.

Sheriff, R.E., 1991, Encyclopedic dictionary of exploration geophysics: Tulsa, Oklahoma, Society of Exploration Geophysicists, Geophysical References Series 1, 376 p.

Shoemaker, E.M., Squires, R.I., and Abrams, M.J., 1978, Bright Angel and Mesa Butte Fault systems of northern Arizona, *in* Smith, R.B., and Eaton, G.P., eds., Cenozoic Tectonics and Regional Geophysics of the Western Cordillera: Geological Society of America Memoir 152, p. 341–367.

Sorauf, J.E., and Billingsley, G.H., 1991, Members of the Toroweap and Kaibab Formations, Lower Permian, Northern Arizona, and Southwestern Utah: Rocky Mountain Association of Geologists, The Mountain Geologist, v. 28, no. 1, p. 9–24.

Spies, B.R., and Frischknecht, F.C., 1991, Electromagnetic sounding, *in* Nabighian, M.N., ed., Electromagnetic Methods in Applied Geophysics: Tulsa, Oklahoma, Society of Exploration Geophysicists, Investigations in Geophysics no. 3, v. 2, part A, p. 285–407.

Strangway, D.W., Swift, C.M., Jr., and Holmer, R.C., 1973, The application of audio-frequency magnetotelluric (AMT) to mineral exploration: Geophysics, v. 38, no. 1, p. 139.

Taylor, R.W., 1984, The determination of joint orientation and porosity from azimuthal resistivity measurements, *in* Nielsen, D.M., and Curl, Mary, eds., Proceedings of the National Water Well Association and U.S. Environmental Protection Agency Conference on Surface and Borehole Geophysical Methods in Ground-Water Investigations: Worthington, Ohio, National Water Well Association, San Antonio, Texas, February 7–9, 1984, p. 37–49.

Taylor, R.W., and Fleming, A.H., 1988, Characterizing jointed systems by azimuthal resistivity surveys: Groundwater, v. 26, no. 4, p. 464–474.

Teichert, Curt, 1968, Stratigraphic nomenclature in Devonian of central Arizona: The Mountain Geologist, v. 5, no. 4, p. 179–180.

Thiele, H.J., 1964a, Groundwater hydrological survey—Deep aquifers: Williams, Arizona, City of Williams consultant report, 30 p.

____1964b, Groundwater survey report within 3-mile radius—Shallow aquifers: Williams, Arizona, City of Williams consultant report, 73 p.

Thomsen, B.W., 1969, Surface-water supply for the City of Williams, Coconino County, Arizona: U.S. Geological Survey unnumbered report, 50 p.

Ulrich, G.E., Billingsley, G.H., Hereford, Richard, Wolfe, E.W., Nealey, L.D., and Sutton, R.L., 1984, Map showing geology, structure, and uranium deposits of the Flagstaff 1°x2° quadrangle, Arizona: U.S. Geological Survey Miscellaneous Investigations Series Map I–1446, 1:250,000.

Vozoff, Keeva, 1986, Magnetotelluric methods: Society of Exploration Geophysicists, Geophysics, Reprint Series No. 5, p. 763.

____1991, The magnetotelluric method, *in* Nabighian, M.N., ed., Electromagnetic Methods in Applied Geophysics: Tulsa, Oklahoma, Society of Exploration Geophysicists, Investigations in Geophysics, No. 3, v. 2, part B, chap. 8, p. 641–712.

Wenner, Frank, 1915, A method of measuring earth resistivity: Washington, D.C., U.S. Department of Commerce, Bureau of Standards Bulletin 12, Paper 258, p. 469–478.

Western Region Climate Center, City of Williams precipitation data 1897–1996: Reno, Nevada, Desert Research Institute, at URL http://www.wrcc.dri.edu, accessed 1996.

Wolfe, E.W., Ulrich, G.E., Holm, R.F., Moore, R.B., and Newhall, C.G., 1987, Geologic map of the central part of the San Francisco volcanic field, north-central Arizona: U.S. Geological Survey Miscellaneous Field Studies Map, MF–1959, 1:50,000.

Zohdy, A.A.R., and Bisdorf, R.J., 1989, Programs for the automatic processing and interpretation of Schlumberger sounding curves in QuickBASIC 4.0: U.S. Geological Survey Open-File Report 89–0137–A, 64 p.

Page 38, Blank

SUPPLEMENTAL DATA

Page 40, Blank

Table 3. Data from audiomagnetotelluric and square-array resistivity sites, and estimated water levels near Williams, Arizona

[Minus sign on longitude indicates west longitude; N/A, not applicable]

Site number (See figure 1)	Sounding name	Latitude (decimal)	Longitude (decimal)	Sounding altitude, in meters	Estimated depth to water, in meters	Estimated altitude of water table, in meters
			Tensor soundings			
2	EMI-2	35.2042	-112.2683	2,027	750	1,277
3	EMI-3	35.2494	-112.0831	2,125	850	1,275
4	EMI-4	35.1642	-112.1581	2,140	800	1,340
5	EMI-5	35.1542	-112.1703	2,190	775	1,415
6	EMI-6	35.2753	-112.1108	2,130	900	1,230
7	EMI-7	35.3169	-112.1536	2,030	1,025	1,005
8	EMI-8	35.3133	-112.1925	2,020	900	1,120
9	EMI-9	35.2611	-112.2239	2,253	850	1,403
10	EMI-10	35.2642	-112.2642	2,140	1,300	840
11	EMI-11	35.2067	-112.2641	2,066	650	1,416
12	EMI-12	35.2392	-112.3031	2,006	750	1,256
13	EMI-13	35.1936	-112.0794	2,194	950	1,244
14	EMI-14	35.3319	-112.2347	1,933	1,025	908
15	EMI-15	35.4192	-112.3142	1,864	1,050	814
16	EMI-16	35.4275	-112.2975	1,779	850	929
17	EMI-17	35.4292	-112.2853	1,872	1,000	872
18	EMI-18	35.2772	-112.2175	2,101	725	1,376
19	EMI-19	35.1144	-112.2358	1,986	900	1,086
20	EMI-20	35.1258	-112.2697	1,997	800	1,197
21	EMI-21	35.1453	-112.2977	2,095	775	1,320
22	EMI-22	35.2231	-112.1239	2,152	900	1,252
23	EMI-23	35.1733	-112.1181	2,205	750	1,455
24	EMI-24	35.1703	-112.1839	2,079	850	1,229
25	EMI-25	35.1714	-112.2117	2,218	875	1,343
26	EMI-26	35.2939	-112.1292	2,075	800	1,275
			Scalar soundings			
27	Poquette Homestead	35.2028	-112.1278	2,139	700	1,439
28	Airport Road	35.2933	-112.1926	2,030	500	1,530
29	A-1 well	35.2500	-112.1217	2,135	850	1,285
30	Kaibab Lake	35.2703	-112.1542	2,145	600	1,545
31	Lost Canyon	35.2281	-112.1733	2,150	700	1,450
32	FS124 and P	35.2833	-112.2394	2,090	900	1,190
33	Siever F	35.1936	-112.1681	2,190	800	1,390
34	APR1-40	35.2625	-112.1867	2,060	950	1,110
35	John's H	35.2467	-112.2272	2,063	600	1,463
36	Valle	35.6456	-112.1375	1,826	800	1,026
37	McDougal Flat	35.2119	-112.0672	2,086	900	1,186
38	FS122 and 108	35.1603	-112.2875	1,950	450	1,500
39	FS122 and 42	35.1494	-112.2450	1,995	700	1,295
			Square-array resistivity soundings			
N/A	Poquette Homestead	35.2028	-112.1278	2,139	1,000	1,139
N/A	Airport Road	35.3125	-112.1836	2,005	500	1,505
N/A	McDougal Flat	35.2119	-112.0672	2,086	940	1,146
N/A	Bard Spring	35.2042	-112.2683	2,027	1,000	1,027